Climate change research and action must look beyond 2100
(version 15.12.2020)

Christopher Lyon[1*], Erin E. Saupe[2], Christopher J. Smith[1,3], Daniel J. Hill[1], Andrew P. Beckerman[4], Lindsay C. Stringer[5], Robert Marchant[5], James McKay[6], Ariane Burke[8], Paul O'Higgins[9], Alexander M. Dunhill[1], Bethany J. Allen[1], Julien Riel-Salvatore[8] and Tracy Aze[1]

[1] School of Earth and Environment, University of Leeds, Leeds LS2 9JT, UK
[2] Department of Earth Sciences, University of Oxford, Oxford, OX1 3AN, UK
[3] International Institute for Applied Systems Analysis (IIASA), Laxenburg, Austria
[4] Department of Animal and Plant Sciences, University of Sheffield, Sheffield S10 2TN UK
[5] Department of Environment and Geography, University of York, York, YO10 5NG UK
[6] School of Chemical and Process Engineering, University of Leeds, Leeds, LS2 9JT UK
[8] Département d'Anthropologie, Université de Montréal, Montréal, QC, H3C 3J7, Canada
[9] Department of Archaeology and Hull York Medical School, University of York, York, YO10 5DD UK

* Corresponding author, c.lyon@leeds.ac.uk

Climate change research and action must look beyond 2100

Christopher Lyon[1*], Erin E. Saupe[2], Christopher J. Smith[1,3], Daniel J. Hill[1], Andrew P. Beckerman[4], Lindsay C. Stringer[5], Robert Marchant[5], James McKay[6], Ariane Burke[8], Paul O'Higgins[9], Alexander M. Dunhill[1], Bethany J. Allen[1], Julien Riel-Salvatore[8] and Tracy Aze[1]

[1] School of Earth and Environment, University of Leeds, Leeds LS2 9JT, UK
[2] Department of Earth Sciences, University of Oxford, Oxford, OX1 3AN, UK
[3] International Institute for Applied Systems Analysis (IIASA), Laxenburg, Austria
[4] Department of Animal and Plant Sciences, University of Sheffield, Sheffield S10 2TN UK
[5] Department of Environment and Geography, University of York, York, YO10 5NG UK
[6] School of Chemical and Process Engineering, University of Leeds, Leeds, LS2 9JT UK
[8] Département d'Anthropologie, Université de Montréal, Montréal, QC, H3C 3J7, Canada
[9] Department of Archaeology and Hull York Medical School, University of York, York, YO10 5DD UK

*Corresponding author, c.lyon@leeds.ac.uk

Anthropogenic activity is changing Earth's climate and ecosystems in ways that are potentially dangerous and disruptive to humans[1]. Greenhouse gas concentrations in the atmosphere continue to rise[2], ensuring these changes will be felt for centuries beyond 2100, the current benchmark for prediction[3–6]. Estimating the effects of past, current, and potential future emissions to only 2100 is therefore shortsighted[5]. Critical problems for food production[7,8] and climate-forced 'survival' migration are projected to arise well before 2100[9,10], raising questions regarding the habitability of some regions of the Earth after the turn of the century. To highlight the need for more distant horizon scanning, we model climate change to 2500 under a suite of emission scenarios and quantify associated projections of crop viability and heat stress. Together, our projections show global climate impacts significantly increase after 2100 without rapid mitigation. As a result, projections of climate and its effects on human well-being and associated governance and policy must be framed beyond 2100.

Main

When climate models were first used in the 1980s and 1990s, the year 2100 was seen as a suitably distant horizon for projections. However, this benchmark is now just one human lifespan away, and opportunities to readily curb emissions in line with the Paris Agreement so that global mean temperature remains 'well below' 2°C are rapidly dwindling[1].

Anthropogenic activity is already altering atmospheric carbon dioxide concentrations at a rate exceeding any known in Earth archives over the last 66 million years[11,12], generating changes deleterious for humans and ecosystems[13–15]. Obtaining insights into anthropogenic effects on the Earth system that support human existence is therefore critical for designing governance and policy structures that can mitigate these effects, which are predicted to continue well beyond 2100[16].

Since 1990 the three Working Groups of the Intergovernmental Panel on Climate Change (IPCC) have produced periodic Assessment Reports, including the forthcoming sixth incarnation (AR6; 2021-2022). Projections assessed by the IPCC consider various lines of evidence including palaeoclimate constraints and climate models. Central to future climate projections are socioeconomic scenarios, including estimates of future fossil fuel consumption, land use change, industrial activity, and associated greenhouse gas and short-lived pollutant emissions emissions[16].

The core scenarios prepared for IPCC's Fifth Assessment Report (AR5) were termed Representative Concentration Pathways (RCPs) and covered four emissions trajectories. RCPs ranged from a global scale reduction on fossil fuel reliance and achievement of net-negative CO_2 later this century (RCP 2.6), to a high emissions scenario that included substantial new investments in fossil fuels and lack of global climate policy and governance (RCP8.5)[17]. The newer Shared Socio-Economic Pathways (SSPs) include five development "storylines" that capture emissions scenarios and also pair them with socio-economic scenarios[16,18,19]. However, the primary time horizon for both RCP and SSP scenarios remains at 2100.

It is now clear that without deep and rapid reductions in greenhouse gas emissions, climate change will continue for centuries into the future. Although some climate modelling efforts do project climate beyond 2100[20–22], very few of the latest generation of comprehensive climate models (CMIP6) produce estimates beyond this horizon. Critically, longer-term models are not focussed on predicting aspects of ecosystem services of fundamental importance to human wellbeing, such as habitable land not inundated by sea level rise, suitable regions for agriculture, and availability of freshwater.

In short, although 50 years have passed since the initial climate projections[23], our time horizon for coupled climate projections remains at 2100. Here we present climate projections modelled to 2500 under three emissions scenarios representing strong, moderate and weak global climate policy (RCP2.6, RCP4.5 and RCP6.0). We project crop viability and heat stress as a preliminary view of future food production and temperature habitability after 2100 to highlight the necessity of socio-economic planning on timescales beyond the turn of the next century.

Climate projections and vegetation beyond 2100

To explore the effects of anthropogenic greenhouse gas emissions beyond 2100, RCP scenarios 2.6, 4.5, and 6.0 were run from 1850 CE to 2500 CE (Extended Data Fig. 1) using the HadCM3 atmosphere-ocean coupled climate model[24] linked to the TRIFFID dynamic land surface model[25] (see Methods). HadCM3, despite being developed over twenty years ago, has a long history of robust projections for present-day and palaeoclimate studies[26,27], and a climate sensitivity (3.3°C)[28] representative of the central estimate from AR5 and a recent comprehensive assessment[29]. The effects of climate change on vegetation are captured in our model, but vegetation-induced changes on the land carbon sink do not affect atmospheric CO_2 levels, since the model was run with prescribed greenhouse gas concentrations. Consequently, important Earth-system feedbacks are not

included, possibly rendering estimates of future warming from this model conservative. These include large-scale permafrost thaw and release of CO_2 and CH_4[30], and the influence of Amazon dieback (seen in RCP4.5 and RCP6.0) on the land carbon sink and its capability to absorb excess CO_2[31].

Results of our projections clearly demonstrate that global mean temperature continues to increase after 2100 under all but the low emission RCP2.6 scenario. Under the moderate-high RCP6.0 emissions scenario (a realistic, business-as-usual scenario with low mitigation[32]), global mean warming is 2.2°C above present-day levels by 2100 (Fig. 1, Extended Data Fig. 1) but continues to rise to 3.6°C in 2200 and 4.6°C in 2500. Warming is unequally distributed, with greater warming over the land surface and in polar regions (Fig. 1).

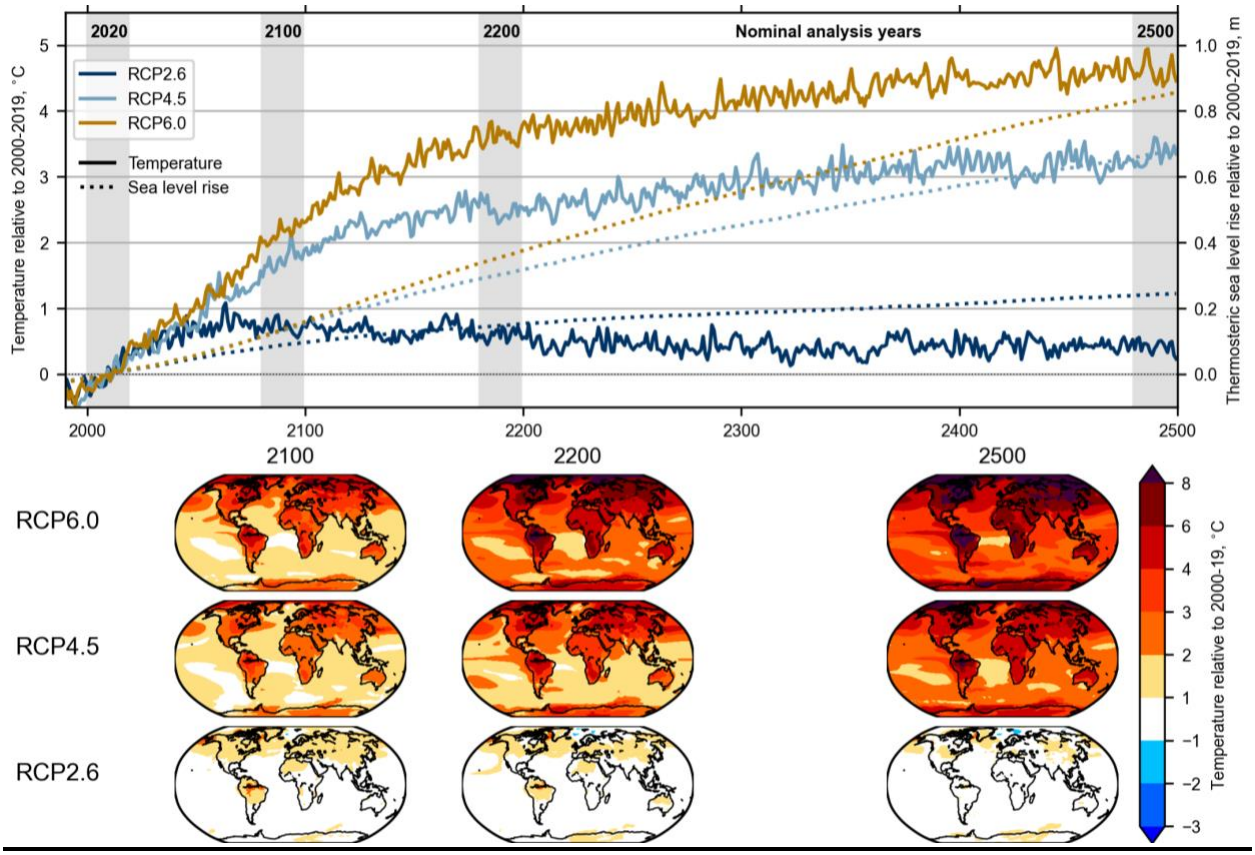

Figure 1. Top panel: Global mean near-surface air temperature (solid lines) and thermosteric sea level rise(dotted lines) anomalies relative to the 2000-2019 mean for the RCP6.0, RCP4.5 and RCP2.6 scenarios. Shaded regions highlight the time horizons of interest and their nominal reference years: 2020 (mean of 2000-19, representative of present-day climate); 2100 (2080-99); 2200 (2180-99) and 2500 (2480-2499). Bottom panel: Spatial anomalies relative to 2000-2019 mean for the 2100, 2200 and 2500 climates under the three RCPs.

The higher emission scenarios (RCP4.5 and 6.0) result in major restructuring of the world's biomes by 2500. For example, HadCM3 projects a severe dieback of Amazon rainforest under RCP6.0 and RCP4.5 by 2500 (Fig. 4), congruent with previous research using the same model under a high emissions scenario[33]. Conversely, the low emissions scenario (RCP2.6) reaches peak warming this century (Fig. 1) with stabilization of global mean temperature only 0.5°C above the 2000-2019 mean and limited long-term shifts in global vegetation (Extended Data Fig. 2). Sea level, however, continues to rise long after warming has stabilised[34], even in the RCP2.6 scenario, due to slow continued mixing of heat into the deep ocean[35] (Fig. 1).

Table 1. Calculated contribution to sea level rise (metres) from deep ocean heat mixing in 2100, 2200, and 2500 under three RCP scenarios

RCP	2100	2200	2500
2.6	0.09 m	0.15 m	0.24 m
4.5	0.15 m	0.32 m	0.68 m
6.0	0.16 m	0.37 m	0.86 m

The long-term impacts of 21st century emissions are therefore likely to be felt for centuries to come, continuing even after greenhouse gas concentrations have reached equilibrium (2150 for RCP4.5 and RCP6.0).

Heat stress and human wellbeing beyond 2100

Heat stress can be fatal to humans when wet-bulb (high humidity) temperatures exceed approximately 35°C within a six-hour measurement interval[36]. Physiologically fit humans can tolerate higher dry-air temperatures, but such temperatures can still lead to high mortalities[37,38]. These conditions also cause damage to critical infrastructure on which humans rely, such as electricity[39], transportation[40], and agriculture[41,42]. Although regional projections of heat stress exist on human comfort[43–45], this body of research does not typically envision thermal conditions beyond 2100.

Here we analyse projected changes in human habitability using the Universal Thermal Climate Index (UTCI)[46] [14,15] (see Methods)—a measure of heat stress encompassing both fatal and physiologically stressful temperatures. UTCI is a single index on a °C scale that reports the effects of climatic conditions on human physiological comfort taking ambient temperature, humidity, solar and thermal radiation, and wind speed into account.

Our measure of UTCI provides an estimate of heat stress levels that are representative of daily near-maximal values (see Methods and Extended Data Fig. 4). The regions that currently experience periods of very strong heat stress today tend to be deserts, but also include the Indian subcontinent and south-eastern US during parts of the year (Fig. 2). Larger proportions of the Earth are projected to experience strong heat stress in the future under RCP4.5 and RCP6.0 scenarios, with affected areas spreading into more temperate zones such as the Mediterranean by the end of the century.

By 2500 under RCP6.0, the proportion of the year exhibiting very strong heat stress is greater than 50% in much of Africa, the Amazon, the Arabian Peninsula, Southeast Asia, the Maritime Continent, and northern Australia. By contrast, today these regions experience this level of heat stress between 0% (Maritime Continent) and 25% (Arabian Peninsula) of the year. Many of these regions are only slightly less affected in RCP4.5 on this timeframe. In contrast, heat stress projections do not become substantially worse beyond 2100 in RCP2.6, showing the long-term advantages of climate mitigation (Fig. 2).

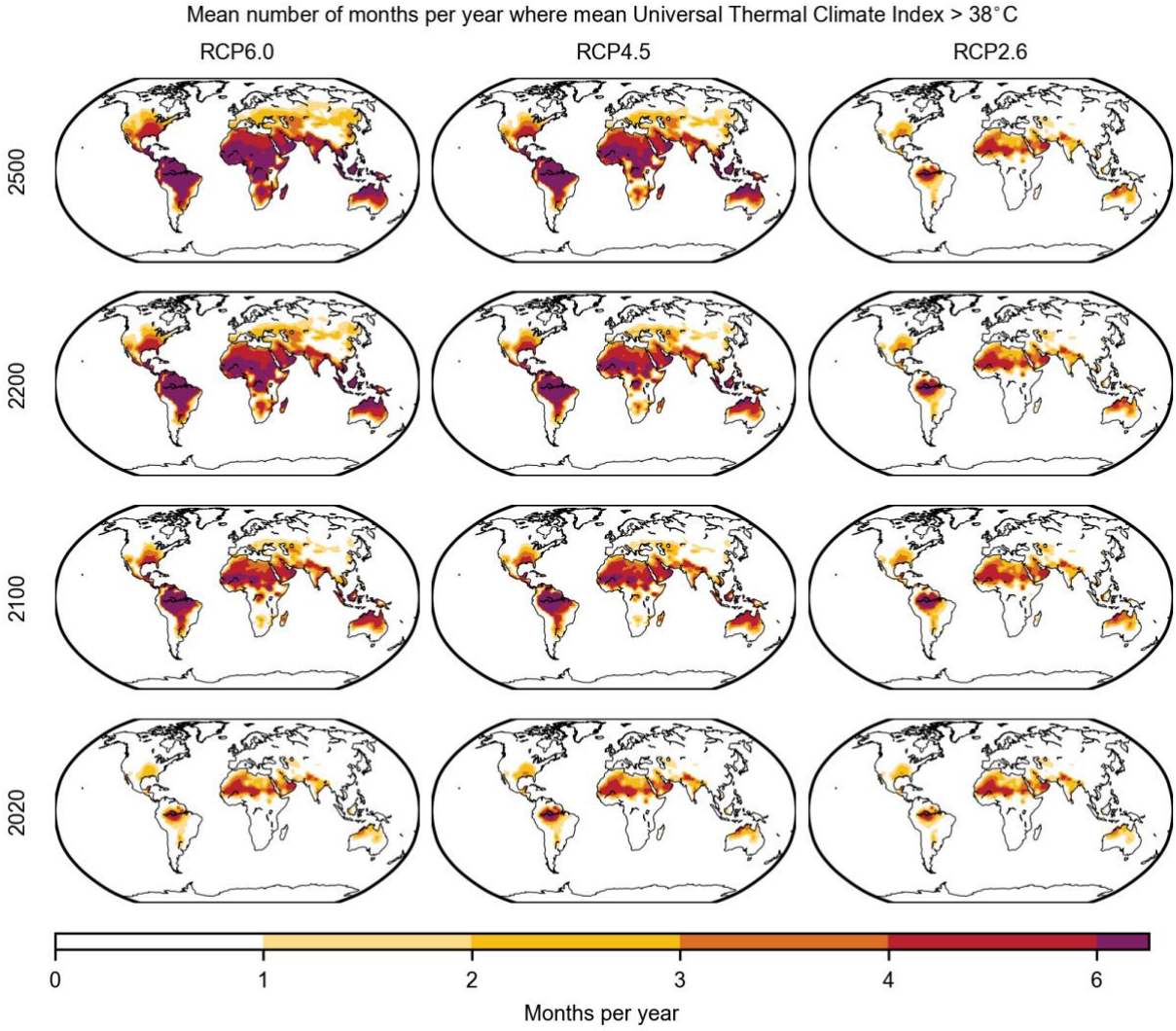

Figure 2. Mean number of months per year where UTCI, a measure of heat stress, exceeds "very strong" levels (38°C on the UTCI scale) in present (2020) and future climates in three RCP scenarios.

High ambient temperatures projected by our models suggest increased periods of physiologically highly stressful, and potentially intolerable, conditions for humans and the infrastructure on which they rely in many parts of the world, including those with high present-day population densities and low indicators of human development[16].

Agricultural challenges after 2100

The effects of climate on agriculture is a major research topic covering crop adaptation, migration, and food production[41,42,47]. Climate-driven crop migration and yield reductions have been observed already[48–50] and projected for the future[51,52], but are not typically projected beyond 2100[53]. Using the climate projections detailed above, we model how future climate change may affect the global extent and location of suitable land for the growth of ten major food crops post 2100[54] (Extended Data Table 1): cassava, maize, potato, rice, sorghum, soy beans, sweet potato, taro, wheat, and yam. Our modelling approach only considered the effect of temperature and precipitation on crop viability, providing a skeleton framework for integrating more sophisticated crop growth measures under projections of longer-term climate conditions. We did not consider how technological and crop innovations and altered land use norms may change viability patterns, nor do we consider factors such as soil depth, soil texture, soil organic matter, soil pH, nutrient availability, biotic symbionts, animal agriculture, pollinators, pests, and diseases, which would improve predictions and even provide estimates of yield.

For each crop, we projected changes to suitable regions for crop growth under future climate scenarios using temperature and precipitation tolerances derived from the Crop Ecological Requirements Database (Ecocrop) of FAO[54] (Extended Data Table 1). Three growing season lengths for each crop were considered due to varying times to crop maturity[73] (Methods). We quantified potential broad scale shifts in where crops can be grown globally by calculating changes in the centroid of suitable crop growth regions (Methods).

These speculative investigations into the potential effects of climate change on crop growth suggest declines in suitable crop growth regions and shifts in where crops can be grown globally (Fig. 3). By 2100 under RCP6.0, we predict declines in land area suitable for crop growth of 2.3% (±6.1%) for staple tropical crops (cassava, rice, sweet potato, sorghum, taro, and yam) and 10.9% (±24.2%) for stable temperate crops (potato, soya beans, wheat, and maize), averaged across crop

growth-length calibrations (Fig. 3; Supplementary Table 1; see Extended Data Figs. 8-15 for additional RCP scenarios). By 2500, declines in suitable regions for crop growth are projected to reach 14.9% (±16.5%) and 18.3% (±35.4%) for tropical and temperate crops, respectively (Fig. 3; Supplementary Table 2). These changes represent an additional six-fold decline in temperate crops and a near doubling of decline for tropical crops between 2100 and 2500. By contrast, if climate mitigation is assumed under RCP2.6, a decline of only 2.9% (±13.5%) is projected by 2500 for temperate crops, and an increase of 2.9% (±3.8%) is predicted for tropical crops.

Declines in suitable regions for crop growth are the dominant pattern projected under future emission scenarios, but considerable variation is found in crop-specific responses (Fig. 3). Wheat, potato, and cassava are projected to lose the greatest area for crop growth by 2500 (Fig. 3; Supplementary Table 2) under RCP6.0 across crop-growth calibrations. Conversely, soya beans and maize are the only crops consistently projected to maintain or gain suitable area under RCP6.0 by 2500 across crop-growth calibrations (Fig. 3; Supplementary Table 2).

Significant changes are also predicted in the locations for staple crop growth. Suitable regions are projected to shift poleward for both hemispheres, although greater shifts are projected in the Northern Hemisphere (Fig. 3). For example, by 2500 under RCP6.0, suitable regions for crop growth are projected to shift by 8.0° (± 3.5) latitude (~900 km) and 6.7° (±2.7) latitude (~700 km) for temperate and tropical crops, respectively, in the Northern Hemisphere, averaged across crop growth-length calibrations (Table S3). This contrasts with the 7.3° (±2.1) and 4.4° (±2.3) latitude shifts predicted for temperate and tropical crops, respectively, by 2100. If mitigation is assumed under RCP2.6, shifts in suitable regions for crop growth are projected of 3.8° (±1.2) and 2.2° (±1.5) latitude for temperate and tropical crops, respectively, by 2500.

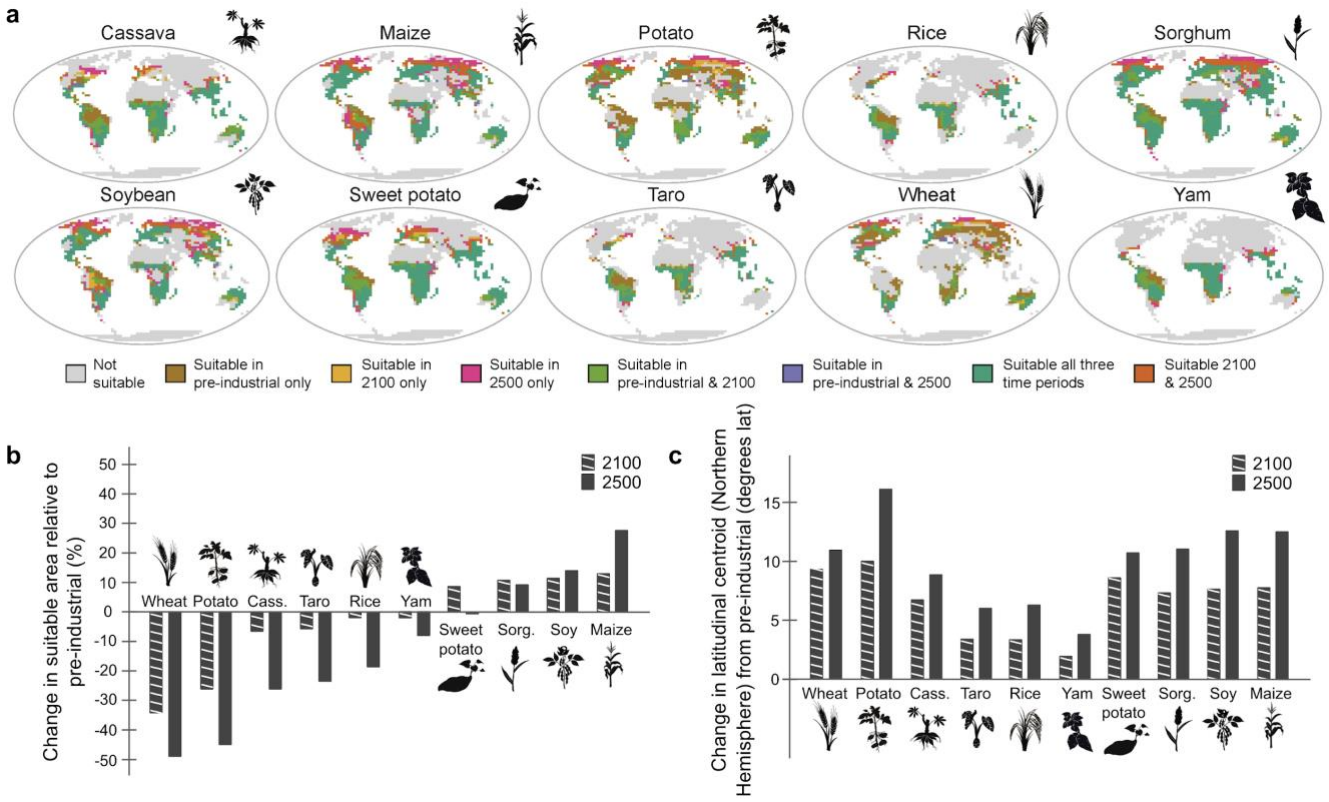

Figure 3. Projections for crop suitability to 2100 and 2500 under the moderate-high RCP6.0 emission scenario. Modelling was based on temperature and precipitation requirements derived from the FAO[54], with crop growth length calibrated to the maps[55] (see Methods). (a) Suitable regions for crop growth globally projected to 2100 and 2500. (b) Projected changes in the area suitable for crop growth globally relative to the pre-Industrial (1851-1899). (c) Projected changes in latitude at which crops can be grown in the Northern Hemisphere, relative to the pre-Industrial (1851-1899). Analyses relied on the latitudinal centroid of suitable crop regions. Cass. = Cassava and Sorg. = Sorghum.

These latitudinal shifts and reductions in suitable area for crop growth in the centuries after 2100 are not accounted for in existing models forecasting food production for future generations. The impacts of these potential changes may be further compounded by changes in human population.

At present, population projections suggest that humans may number anywhere between 7-16 billion by the year 2100[56,57], putting additional strain on models that suggest increasingly scarce food resources and highlighting the urgency of addressing population and food security questions[58–61].

Regional case studies

The changes we have projected are likely to have profound effects not only on natural vegetation but on human society by altering the distribution of tolerable environments and by changing the feasibility of agriculture. To better explore the effect of these changes on human society, we highlight site-specific projections for three regions (Extended Data Fig. 3) of global importance under RCP6.0: the North American "breadbasket", the Amazon basin carbon sink, and the densely-populated Indian subcontinent (Fig. 4; Box 1; see also Extended Data Fig. 5 and 6 for additional RCPs). We use our results to inform artistic interpretations of regional scenes to highlight the profound changes these regions may face under a plausible medium-high emission scenario (RCP6.0)[32] after 2100 (Box 1).

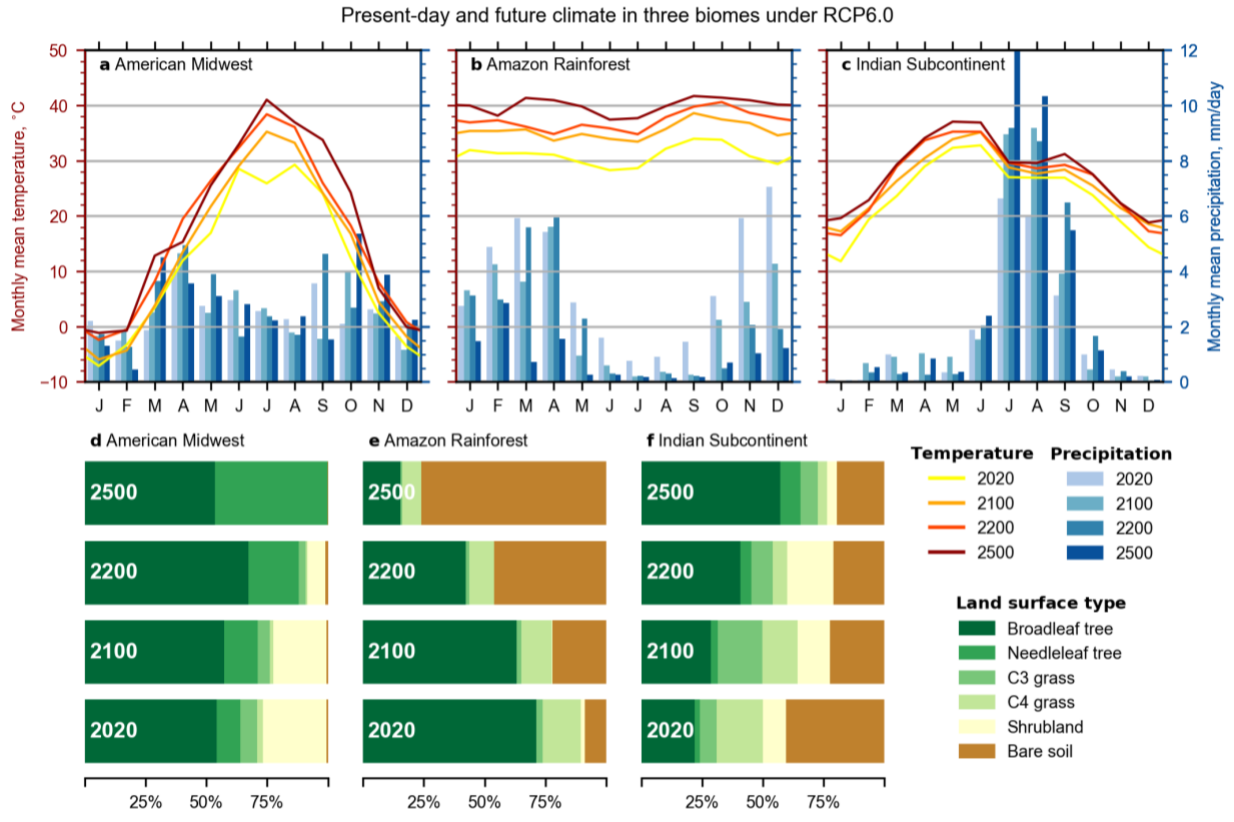

Figure 4. Climatic indices for the three case study regions under the RCP6.0 scenario in HadCM3. Monthly mean temperatures (°C; left axis) and precipitation (mm/day; right axis) in (a) the American Midwest, (b) Amazon and (c) Indian subcontinent. Land cover fractions, from the TRIFFID dynamic vegetation model in (d) American Midwest, (e) Amazon and (f) Indian subcontinent.

North American Midwest. The interior plains of the American 'Midwest' (roughly present-day US states of Illinois, Indiana, Iowa, Michigan, Minnesota, Ohio, and Wisconsin; Extended Data Fig. 3) are a global breadbasket. Today the Midwest is characterised by cold winters and warm summers[62]. Under RCP6.0, mean summertime temperatures increase from 28°C today to 33°C by 2100 and 36°C by 2500 (Fig. 4). Heat stress (measured with UTCI) increases in line with ambient temperature: 34.8°C in the warmest month today to 39.8°C in 2100, 42.9°C in 2200, and 44.9°C in 2500. With a definition of "very strong heat stress" at UTCI > 38°C[46], such a seasonal climate approaches levels that are physically stressful to intolerable for humans and many other species.

Amazon basin. The Amazon Basin is home to one third of Earth's known species [63] and currently serves as a carbon sink for roughly 7% of anthropogenic CO_2 emissions[31,64] (Extended Data Fig. 3). The region is also diverse culturally and linguistically, home to more than 350 indigenous languages[65]. Our modelling suggests that rising temperatures and disrupted rainfall patterns will render the Amazon Basin unsuitable for tropical rainforests by 2500 (Fig. 4, Box 1), with consequences for the global carbon cycle, biodiversity, and cultural diversity. Initial declines in forest cover in the model lead to a positive feedback of reduced transpiration, further reduced rainfall, and further forest retreat. The HadCM3 climate model exhibits this feedback more than most climate models, especially in the Amazon Basin[66,67], but still has a plausible sensitivity[68]. The newer HadGEM2-ES model also shows Amazon dieback (though less severe), with freely-evolving vegetation when run to 2300AD under a high emissions scenario[69]. The model projects a limited retreat of the Amazon rainforest by 2100, but in the following centuries, forest dieback feedback enhances forest loss, and high temperatures and low precipitation conspire to produce a barren environment in most of the Amazon Basin. Amazonian forest cover declines from 71% in the present day to 63% in 2100, 42% in 2200 and 15% in 2500.

Indian subcontinent. The Indian Subcontinent is one of the most populous regions on Earth (Extended Data Fig. 3). The region already experiences extreme climatic conditions, with thousands of heat-stress related deaths recorded between 2013-2015 alone[70]. Our modelling suggests that mean

summer monthly temperatures could increase 2°C by 2100 and 4°C by 2500, suggesting the Indian subcontinent will experience even higher heat stress than those projected by 2100[44] (Fig. 4; Box 1). The dynamic land vegetation model projects tropical forest expansion across the Indian subcontinent towards 2500. Monsoon rainfall is projected to increase substantially into the future, reaching double the rate of precipitation today by 2500 under RCP6.0. Conversely, year-2500 climate and heat stress projections are similar to today under the RCP2.6 mitigation scenario, showing the effect of early reduction in greenhouse gas emissions.

Box 1. Artistic comparison of potential changes in regional landscapes and human activity between 2020 and 2500 under RCP6.0
Three image pairs illustrate the potential scope of regional changes under RCP6.0 (Fig. 4). While technology in 2500 is essentially unknowable, we limited technological advancement for the purposes of making comparisons between 2020 and 2500.

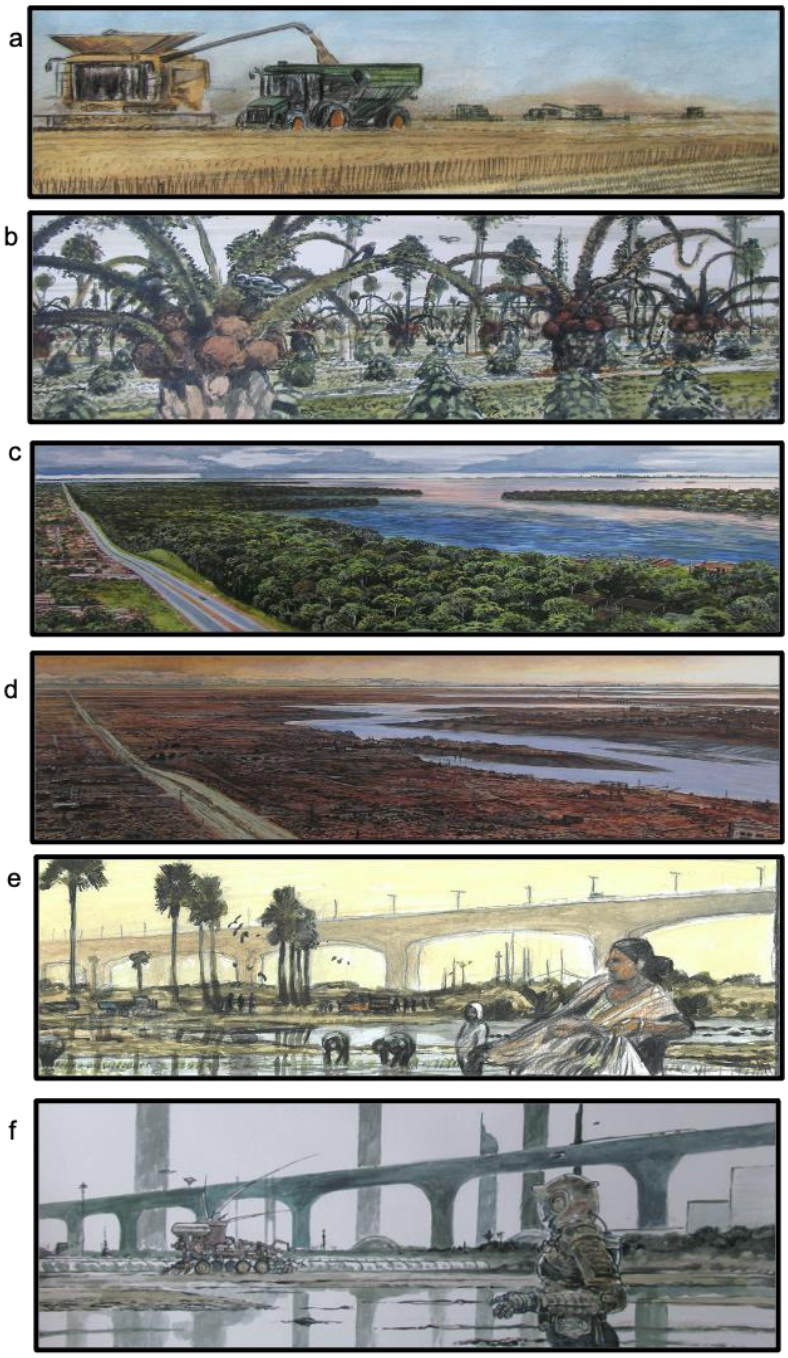

US Midwest Breadbasket (a) 2020 and (b) 2500 under RCP6.0
Scenario A characterisation of the 'breadbasket' area of the US Midwest today and in 2500. In 2500 monocultured cereals may be replaced by a subtropical agroforestry of fictional plants (based on oil palms and arid zone succulents)**.** Potential future water capture and irrigation devices can be glimpsed among the crops to offset the effects of extreme summer heat.

Amazon (c) 2020 and (d) 2500 under RCP6.0 scenario A characterisation of the Amazon today and in 2500. In 2500 forest cover may be largely gone, with reduced surface water levels. Human presence and infrastructure may be minimal, degraded, or absent, given high temperatures and water stress.

Indian subcontinent (e) 2020 and (f) 2500 under RCP6.0 scenario A characterisation of India in the present day and in 2500. We illustrate a conservative view of potential human adaptations based on similar technology today and from science fiction[71,72]. Extreme heat may require protective personal clothing for outdoor activity—in this hypothetical case, a sealed helmet and a suit conducting water and coolants around the body. Outdoor agriculture in 2500 may be managed by automated drone-machinery.

Governance and research for long timescales

Human activity has already caused warming of ~1°C above average global pre-industrial levels[1]. Global mean temperatures will continue to increase unless and until CO_2 emissions reach net zero[73–75]. Return to a pre-industrial climate is not possible without either removal of excess greenhouse gases added to the atmosphere or a sustained geoengineering programme[76]. The latter is unlikely given failures of governance around negative emissions technologies[76–78]. As such, a longer-term post-2100 perspective is critical for assessing the scope of climate change on Earth systems and human well being[79].

Our climate, heat stress, and agricultural projections parallel work suggesting climate increasingly drives global and regional human dispersal[10], especially from the heat-stressed tropics where habitability and crop suitability may be much reduced. The scale of change we project over the coming centuries, especially under RCPs 4.5 and 6.0, will necessitate more cooperative and collaborative approaches to global mobility and migration to accommodate substantial human movement from less habitable regions[9]. Meeting this challenge will require a major evolution in international relations away from national security and competition toward cooperation and integration[80].

Our projections for crop viability also portend declines in ecosystem services after 2100. Even before 2100, projections of climate change suggest low income (tropical) countries are vulnerable to reduced crop suitability, and high income countries face challenges with inward migration and converting climatically-suitable land to agriculture[81–83]. Such shifts also bring risks of soil carbon release, incursion into biodiversity hotspots, and threats to water security[83,84]. Over the long-term, proposed strategies for food security, even those considered transformative[47,85] such as meatless diets and urban farming, may be insufficient if present agricultural areas fall out of production and technological advancements or landscape management (e.g. agroecology) prove unworkable at scale. The structure and function of the global food system will require reimagining,

potentially via changes to property rights, use, and ownership[86] that mirror changes in productive climates, landscapes, populations, and technologies[47,58].

The scope of projected future changes examined here will require long-term and adaptive integration of knowledge and governance structures that are global in scope and approach[87,88]. Indigenous groups, well-situated to assess ecological and human determinants of regional vulnerabilities, should be included in this process[89–91] as they point out[92]. Emerging research shows that plausible and desirable low carbon modes of living are possible[93] but challenging to implement[94], particularly at scale and for billions of people distributed across urban and rural landscapes.

International accords (e.g. Paris Agreement[95]) may have slowed the growth of greenhouse gases in the atmosphere, but commitments still fall massively short of the 1.5°-2.0°C frontier[96]. Such international agreements also depend on the circumstances of nation states and capacities to reduce emissions, which remain fragile, e.g., due to risk of failures to meet targets and over-reliance on presumptive CO_2 removal technologies[78]. Even if such commitments are met, projections still show that we must contend with more frequent heat waves and other extreme events[97,98]. Although the Paris Agreement calls for a progressive ratcheting of emission reductions over time, current levels of Nationally Determined Contributions put us somewhere between RCP4.5 and RCP6.0 scenarios, heralding warming of a further 2°C this century[32,99].

The imperative to reduce greenhouse gas emissions and limit the effects of climate change beyond 2100 requires innovative and visionary decision making[20,28] and cooperation[29,30] that draws on diverse sources of knowledge[100,101]. For example, new knowledge-action synthesis efforts[18,102], such as long-range 'Ministries for the Future'[103], could be tied to existing multilateral or enhanced polycentric institutional frameworks such as the United Nations [32]. Such cross-cultural organisations would evolve to keep ahead of observed and anticipated human migration, food production, disasters, and other climate and ecological challenges [33,34]. Practically, this could mean developing a

rolling-baseline, Russian-doll approach to scenarios and decision making, embedding subjectively short (0 - 50 years) local or regional assessments and actions inside medium (50 - 100 years) and longer-term global perspectives (>100 years) based on observed and modelled impacts and thresholds. This approach to governance would accommodate rapid events, such as floods and droughts, within slower-moving changes to temperature, sea-level, crops and biodiversity. Projections of climate and Earth system changes beyond 2100 can inform these longer-term approaches, helping to ensure changes to ecosystems and their resources are adequately managed to sustain human survival[104].

Moving into the future

The year 2100 is one human lifespan away, and the window to readily curb emissions in line with the Paris Agreement is rapidly closing[105]. Our projections past 2100 indicate that without rapid and significant reductions in greenhouse gas emissions, large areas of the Earth will change in ways that reduce their capacity to support large-scale human occupation. The long-term effects of 21st century warming will be felt for centuries to come, even if emissions are limited in the future (Fig. 1). We therefore need to understand and model these changes beyond the next 80 years. These longer-term projections are critical to preparing the way for a peaceful and habitable Earth in the coming decades and centuries.

The projections presented here represent an initial attempt at longer-term modelling and have considerable uncertainty given their expanded time horizon. These efforts highlight the need for more sophisticated climate and Earth system modelling beyond 2100, including focus on aspects of ecosystem goods and services not considered here. Our work provides a framework and baseline for the assessment of longer-term anthropogenic effects on climate and Earth systems, and highlights the critical need for further work in this area.

Methods

Climate and vegetation projections

HadCM3 climate model The HadCM3 version of the UK Met Office's Unified Model is a fully coupled ocean-atmosphere General Circulation Model (GCM) appearing in various guises in Coupled Model Intercomparison Project (CMIP) phases CMIP2, CMIP3 and CMIP5[106]. HadCM3 has an atmospheric model with a resolution of 3.75° x 2.5° with 19 levels in a hybrid vertical coordinate and an ocean model of 1.25° x 1.25° with 20 levels. These simulations incorporate the TRIFFID Dynamic Global Vegetation Model 37 into the MOSES2.1 land surface scheme [107,108], which is run dynamically coupled to the HadCM3 climate model (HadCM3B-M2.1aD)[109]. HadCM3, despite being a reasonably old model, is representative in terms of its climate sensitivity and climate response to forcing[28], and its lower computational resource compared to newer models allows projections to 2500 to be easily run.

Raw climate model data was not bias-corrected for input into crop and heat-stress projections. As a proxy for observations, we compared to temperature and precipitation using the ERA5 reanalysis[110] from 1979-2019. Analysis shows that a warm bias exists in the Breadbasket region under present-day climate in the summer months of several degrees Celsius, and in the Amazon region year-round. Northern Hemisphere summer land temperatures are also substantially warmer than ERA5. If these spatial warm biases persist as global mean climate changes under the three forcing scenarios, it is possible the UTCI heat stress metric (the variance in which is dominated by ambient air temperature) in these regions may also be biased high in the future. However, the present-day warm bias is due, in part, to the model being run without aerosol and volcanic forcing, and the relative importance of this lack of offset cooling will reduce as aerosol forcing reduces in the RCPs into the future. The model also projects substantially less precipitation than ERA5 in the Amazon region (which may accelerate rainforest dieback in the future projections) and in India,

particularly during the monsoon months. Precipitation (along with temperature) biases may affect crop yield projections.

TRIFFID DGVM The Dynamic Global Vegetation Model (DGVM) [25] component of the MOSES land surface scheme[107,108] simulates five functional types of vegetation: broadleaf tree, needle-leaf trees, C3 grasses, C4 grasses and shrubs. A combination of these functional types is simulated for each of the grid cells, along with barren landscapes where nothing will grow and specified urban, open water and permanent ice fractions. These depend on the climatic impacts on photosynthesis, plant respiration and leaf mortality and competition for light, water and carbon. Carbon fluxes are calculated using a coupled photosynthesis-stomatal conductance model[111]. An allocation scheme distributes carbon between stem, root and leaf components, and a hydrological budget distributes rainfall between canopy, throughfall, soil moisture and runoff. Litter fall increases soil carbon, and microbial respiration returns carbon to the atmosphere[25].

Simulation Design All the simulations are initiated from long pre-industrial simulations and run from 1850 to 2500 CE. The only changes through the transient simulation are the atmospheric concentrations of carbon dioxide, methane, and nitrous oxide, which are based on the Representative Concentration Pathways RCP2.6, RCP4.5 and RCP6.0[112]. These RCP scenarios provide time-dependent projections of atmospheric greenhouse gas concentrations, and represent realistic socio-economic scenarios of strong, moderate and weak climate mitigation and adaptation respectively[17]. An RCP8.5 (high emissions, no mitigation) scenario[113] was started, but model instabilities caused the run to fail. We note that an emissions pathway following RCP8.5 is unlikely, as it would require substantial new investments in fossil fuels[32], but a concentration pathway following something like this trajectory cannot be ruled out if global mitigation action is weak and Earth system feedbacks (such as large-scale permafrost thaw or the reversal of the Amazon carbon sink) are strong.

The model was run without other forcings, including negative forcings from anthropogenically-emitted aerosols and volcanic eruptions. Although this may slightly overstate the

magnitude of pre-industrial to present-day warming in our model results, longer-term projections will be less affected as aerosol emissions undergo a reduction in all RCP scenarios over the course of the 21st century; therefore, future changes from a present-day baseline may be slightly underestimated. Each of these scenarios were originally extended to 2300 CE (Extended Concentration Pathways) under more limited socioeconomic assumptions than modelled to 2100[17]. We use these pathways to 2300 and assume constant atmospheric concentrations between 2300 and 2500. This agrees with the extended RCPs to 2500 CE described by Meinshausen et al[112] for RCP6.0 and RCP4.5, but our treatment of RCP2.6 differs, as we assume constant concentrations unlike the continually declining concentrations in Meinshausen et al[112].

Sea-level rise Sea level rise from the thermal expansion of sea water (Fig. 1) is calculated from the change in ocean heat content in YJ multiplied by 0.114 m YJ^{-1}, the thermal expansion coefficient for HadCM3[114]. As other components of sea level rise, such as ice melt from glaciers and the Greenland and Antarctic ice sheets, cannot be easily determined and are generally not estimated from global climate models, our projections are likely to be conservative.

Region definitions Case-study regions are given in Extended Data Fig. 3 and were chosen as representatives of diverse physical (climate, landscape, vegetation) and human (population, human development or income level, ecosystem services, agricultural productivity) regions of Earth. The North American "breadbasket" was defined to be approximately coincident with the present-day US states of Illinois, Indiana, Iowa, Michigan, Minnesota, Ohio, and Wisconsin, comprising the region 40-47.5°N, 81.25-97.5°W, and did not include the portion of this rectangle northeast of the Great Lakes in the Canadian province of Ontario. The Amazon region was defined to be the same region used in Huntingford et al (2008)[33] in their consideration of Amazonian forest loss in the HadCM3 model, a non-rectangular region covering 12.5°S - 5°N and 71.25°W-41.25°W. The Indian Subcontinent region was based on the definition of the South Asia climatic zone[115], with a more restricted horizontal domain (5-30°N, 67.5-90°E) covering approximately the countries of Pakistan,

Nepal, India west of the Bay of Bengal and south of 30°N, and the western portions of Bhutan and Bangladesh. In all cases, climatic results are only reported for land grid cells.

Heat stress

A proxy for heat stress on human physiology is calculated using the Universal Thermal Climate Index (UTCI) [46,116]:

$$T_{\mathrm{UTCI}} = f(T_{\mathrm{s}}, T_{\mathrm{mrt}}, w, h_{\mathrm{rel}})$$

where f is a sixth-order polynomial function of near-surface air temperature (T_{s}), mean radiant temperature (T_{mrt}), 10m wind speed (w) and relative humidity (h_{rel}), using the FORTRAN code available from http://www.utci.org/public/index.php?dir=UTCI+Program+Code%2F [117]. Climatic outputs are taken directly from HadCM3. 10m wind speed is calculated as $w = \sqrt{u^2 + v^2}$ where u and v are the westerly and southerly wind components from HadCM3.

T_{mrt} represents the effective temperature of the radiation received from a body due to its surroundings. The conversion from radiation to a measure of temperature follows from the Stefan-Boltzmann equation and is calculated following Di Napoli et al.[118] (and references therein):

$$T_{\mathrm{mrt}} = \left(\frac{1}{\sigma} \left(f_{\mathrm{sky}} L_{\downarrow} + f_{\mathrm{ground}} L_{\uparrow} + \frac{a_{\mathrm{ir}}}{\epsilon_{\mathrm{p}}} \left(f_{\mathrm{sky}} S_{\downarrow,\mathrm{diff}} + f_{\mathrm{ground}} S_{\uparrow} + \frac{f_p S_{\downarrow,\mathrm{dir}}}{\cos \theta_z} \right) \right) \right)^{\frac{1}{4}}$$

where σ is the Stefan-Boltzmann constant (5.67×10^{-8} W m^{-2} K^{-4}), $f_{\mathrm{sky}} = f_{\mathrm{ground}} = 0.5$ is the fraction of total radiation emanating from the sky and ground respectively, $\alpha_{\mathrm{ir}} = 0.7$ and $\epsilon_{\mathrm{p}} = 0.97$ are the infrared absorption and emissivity of the clothed human body, respectively, L and S represent

surface-level longwave and shortwave (solar) horizontal radiation fluxes, and subscripts ↓, ↑, diff and dir represent downwelling, upwelling, diffuse and direct fluxes, respectively [118]. The time-averaged cosine of the daytime solar zenith angle $\overline{\cos\theta_z}$ is calculated for each latitude point and month using the Met Office Unified Model FORTRAN subroutines offline[109].

The surface projection factor describes the proportion of the human body that is intercepted by the incoming direct radiation [119], described empirically by Di Napoli et al.[118](and references therein):

$$f_{\mathrm{p}} = 0.308\cos\left(\left(\frac{\pi}{2} - \bar{\theta}_z\right)\left(0.998 - \frac{\left(\frac{\pi}{2} - \bar{\theta}_z\right)^2}{50000}\right)\right)$$

Model-derived direct and diffuse shortwave fluxes were not saved from HadCM3, so the diffuse fraction of monthly mean downwelling surface radiation is estimated from the monthly mean clearness index $\overline{K_{\mathrm{T}}}$ [120,121]:

$$\frac{S_{\downarrow,\mathrm{diff}}}{S_{\downarrow}} = \begin{cases} 1.391 - 3.560\overline{K_{\mathrm{T}}} + 4.189\overline{K_{\mathrm{T}}}^2 - 2.137\overline{K_{\mathrm{T}}}^3 & \omega_s \leq 1.4208 \\ 1.311 - 3.022\overline{K_{\mathrm{T}}} + 3.424\overline{K_{\mathrm{T}}}^2 - 1.821\overline{K_{\mathrm{T}}}^3 & \omega_s > 1.4208 \end{cases}$$

where $\overline{K_{\mathrm{T}}}$ is the ratio of surface to top-of-atmosphere horizontal shortwave radiation flux from HadCM3, and the sunset angle ω_s is calculated from latitude ϕ and monthly-mean solar declination δ:

$$\cos\omega_s = -\tan\phi\tan\delta$$

Our metric for reporting heat stress in Fig. 2 is the proportion of months where mean UTCI exceeds 38°C, defined as "very strong heat stress" [46].

Although UTCI is designed to be an instantaneous metric, we find that calculating it with monthly mean climatic data does not lead to unreliable results (Extended Data Fig. 2). To conduct this test, UTCI from the three case study regions was compared using 3-hourly climate model data alongside monthly climate data from the HadGEM2-ES model for the year 1985. From the 3-hourly data, diffuse radiation is available from the model directly and used instead of the method based on monthly mean clearness index. We find that UTCI calculated from monthly mean data is near the upper range of the daily maximum values from the 3-hourly data but generally does not exceed it, suggesting that monthly UTCI is a good indicator of typical daily high values (but not extreme highs) in a particular month.

Crop projections

Projections of crop viability under future climate scenarios have been conducted, but efforts remain confined to the 2100 time horizon [122,123]. Building on established methods of predictive future agriculture modelling [124–130], we assessed the degree to which predicted future climate change may affect the amount and location of suitable area for growth of leading food crops. We focused on 10 crops that are grown globally and feed a large portion of the human population: cassava, potato, soya bean, rice, sweet potato, sorghum, taro, wheat, yam, and maize (Food and Agricultural Organization of the United Nations [54] (Extended Data Table 1). Analyses were conducted on a gridded world of 417 km x 272 km resolution. For each crop, we assessed whether climatic conditions for a cell were suitable for crop growth in pre-Industrial times (1851-1899), comparing these maps of suitability to conditions derived from the HadCM3 coupled atmosphere-ocean climate model run at 3.75° x 2.5° resolution (Methods), using the three RCPs, 2.6, 4.5 and 6.0 [17,131,132]. Climatic conditions for the pre-

Industrial (1851-1899), 2100 (2080-2099), and 2500 (2480-2499) were extracted from the simulations in the form of mean annual precipitation (mm/year) and mean monthly temperature (°C).

Crop tolerances Temperature and precipitation tolerances for crops were derived from the Crop Ecological Requirements Database (Ecocrop) of FAO[54] (Extended Data Table 1). This database provides information on crop cycle and predicts crop viability in different climatic conditions in different Earth regions. We characterized crop tolerances using acceptable/marginal climatic ranges from the database, rather than optimal climatic ranges, as this approach allowed for the greatest extent for crop growth globally and therefore represents a 'best-case' scenario for future food production.

Crop suitability For a given crop, we assessed whether the temperature and precipitation conditions for each grid cell on Earth were suitable for the length of a growing season. The length of the growing season was considered in months, converted from days in Ecocrop (Extended Data Table 1). Suitability of grid cells was determined using three growing season lengths: minimum, maximum, and calibrated to crop growth based on global cropland maps[55].

To calibrate the length of growing season based on global crop harvest, we estimated crop suitability (see below) under pre-Industrial conditions for each growing month inclusive of the minimum to maximum months. Suitability maps were compared to crop growth maps globally[55]. Crop growth maps were coarsened to the resolution of the climate model (3.75° x 2.5°) and converted to binary (crop grown *versus* not grown) if any fraction of a cell was harvested for the given crop. Estimated suitability maps were compared to global crop growth maps using measures of omission (crops grown in grid cells but grid cells not estimated as suitable) and commission (grid cells estimated as suitable but crops not grown in grid cells). The growing length associated with the modelled suitability map that best minimized omission and, secondarily, commission, was used for the 'calibrated growing cycle length' (Extended Data Table 1). Areas of omission were prioritized

over areas of commission because these grid cells are known to be suitable for crop growth but models did not predict them as such, whereas areas of commission may result for reasons other than suitability (e.g., geopolitical, knowledge gaps, etc.). In spite of close agreement and low omission scores between crop suitability models and crop growth maps, a few crops were underpredicted in our modelling: potato, soybeans, wheat and maize in northwest South America, yam in the Middle East, taro in Spain and the Middle East, and rice in India and the Middle East.

Two requirements needed to be met for a given grid cell to be suitable for a crop: (i) the mean monthly temperature of the grid cell was within the acceptable range for a *consecutive* number of months, corresponding to the maximum, minimum or calibrated growing cycle length. In this way, we accounted for the number of growing days needing to be suitable for crop growth; and (ii) the grid cell value for annual precipitation was within the acceptable range. Analyses were conducted using a custom script in the R programming language[133], which called on functions in the 'bnspatial' v1.1.1 [134] and 'raster' v.3.1-5 [135] packages.

Each grid cell was deemed suitable or unsuitable for crop growth for each time (pre-Industrial, 2100, and 2500) by growth cycle length (maximum, minimum, and calibrated) by RCP scenario (2.6, 4.5, and 6) and crop combination. We quantified the proportion of terrestrial area suitable globally for each combination using equal-area grid cells (417 km x 272 km) based on the Lambert World Cylindrical Equal Area map projection.

Latitudinal shifts in crops To quantify broad-scale shifts in the area suitable for crop growth, we calculated the centroid of suitable cells for each combination and tracked changes in these centroids through time. The raster grid of suitable conditions for each combination was converted to a polygon and all sub-geometries discarded using the 'raster' v.3.1-5 package [135] for R. The centroid of the suitable polygons was measured using the gCentroid() function in the 'rgeos'

v.0.5-3 [136] package for R. Analyses were performed independently for Northern and Southern Hemispheres.

Modelling caveats

Our modelling is not as complicated as many detailed crop-specific exercises, which are often process-based and include growth parameters and soil and nutrient conditions [137]. Analyses of suitable regions for crop growth relied only on coarse-scale temperature and precipitation conditions derived from a coupled atmosphere-ocean simulation, HadCM3. Our analyses additionally assumed crops were grown in natural conditions, not in environmentally controlled facilities, and no technological advances in crop development occurred[138]. Our predictions do not account for changes in crop tolerance, which could allow for growth of crops in conditions different to those considered here.

We also do not consider factors such as soil depth, soil texture, soil organic matter, soil pH, nutrient availability, biotic symbionts, animal agriculture, pollinators, pests, and diseases, which influence where crops can grow. The inclusion of these factors will likely improve model predictions[130]. Our models may be best case scenarios for high latitudes, since there is very little research on the viability of large scale circumpolar agriculture in available soil types, including potential for CO_2 release[83]. These variables were not included in our modelling exercise because they are difficult to project into the distant future (i.e. 2500), and are not well represented by the coarse spatial scale of our analyses (i.e. they are heterogenous at finer spatial scales).

Other assumptions of our crop modelling include counting all regions within a grid cell as suitable. Land use, however, is heterogeneous, particularly at the coarse resolution of our analysis and will likely change in the future. We calibrate present-day tolerances based on the atmosphere-ocean climate model using pre-industrial conditions. That said, estimates of where crops can grow in pre-Industrial times are largely congruent with maps of where crops are cultivated today [55,139,139,140].

Finally, we do not account for changes in the amount of terrestrial land area for crop growth in the future, which is likely to diminish due to sea-level rise[141].

Extended Data

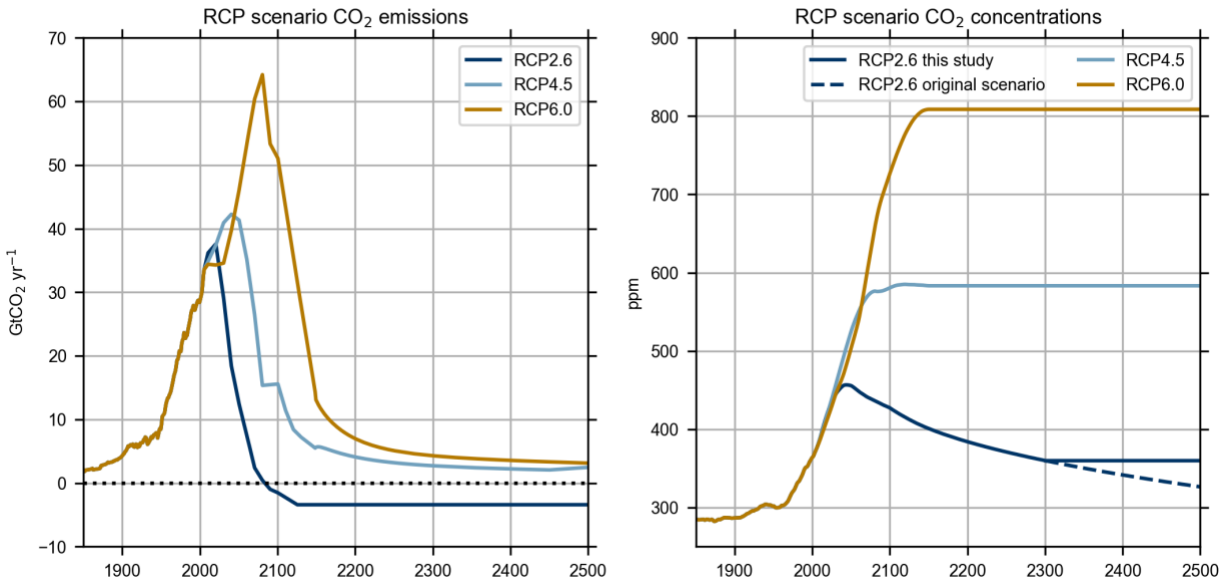

Extended Data Figure 1: Emissions and concentrations of CO_2 in RCP2.6, RCP4.5 and RCP6.0. We use constant CO_2 concentrations for RCP2.6 after 2300 (solid line); the original scenario has continually declining concentrations (dashed line) in response to continuous negative emissions. Data are from Meinshausen et al. (2011)[112].

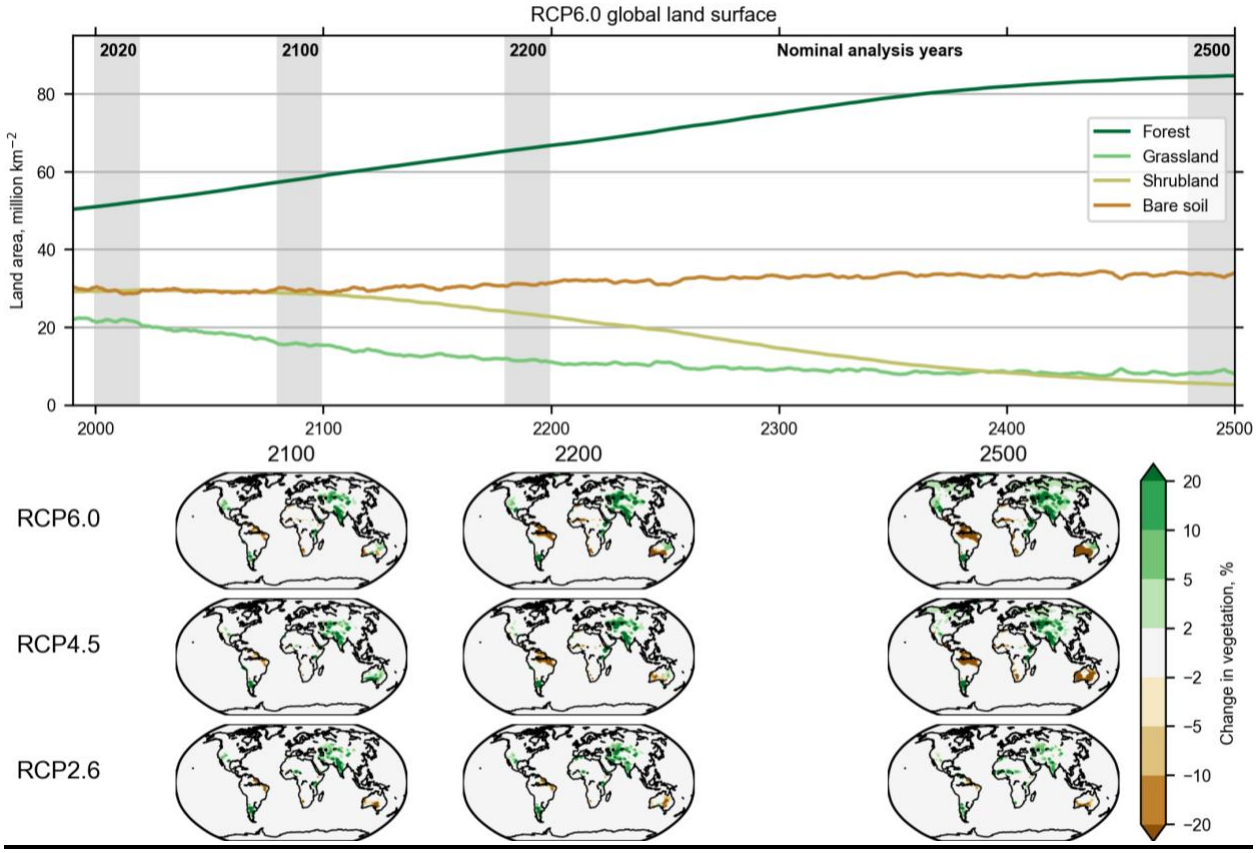

Extended Data Figure 2: Top panel: total land area (million km^2) covered with forest (dark green), grassland (light green), shrubland (yellow) and bare soil (brown) in the TRIFFID DGVM component of HadCM3 under the RCP6.0 scenario. Bottom panel: Regional changes in vegetation fraction (total of forest, grassland and shrubland, expressed in %) of land surface (green) versus bare soil (brown) for 2100, 2200 and 2500 compared to present day.

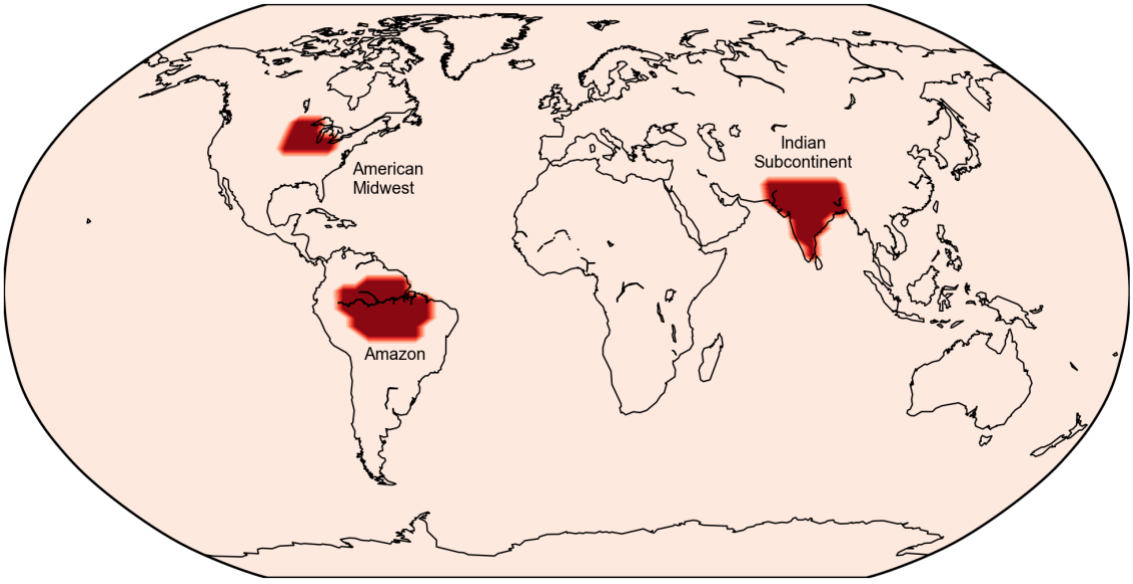

Extended Data Figure 3: Global locations of the case study regions.

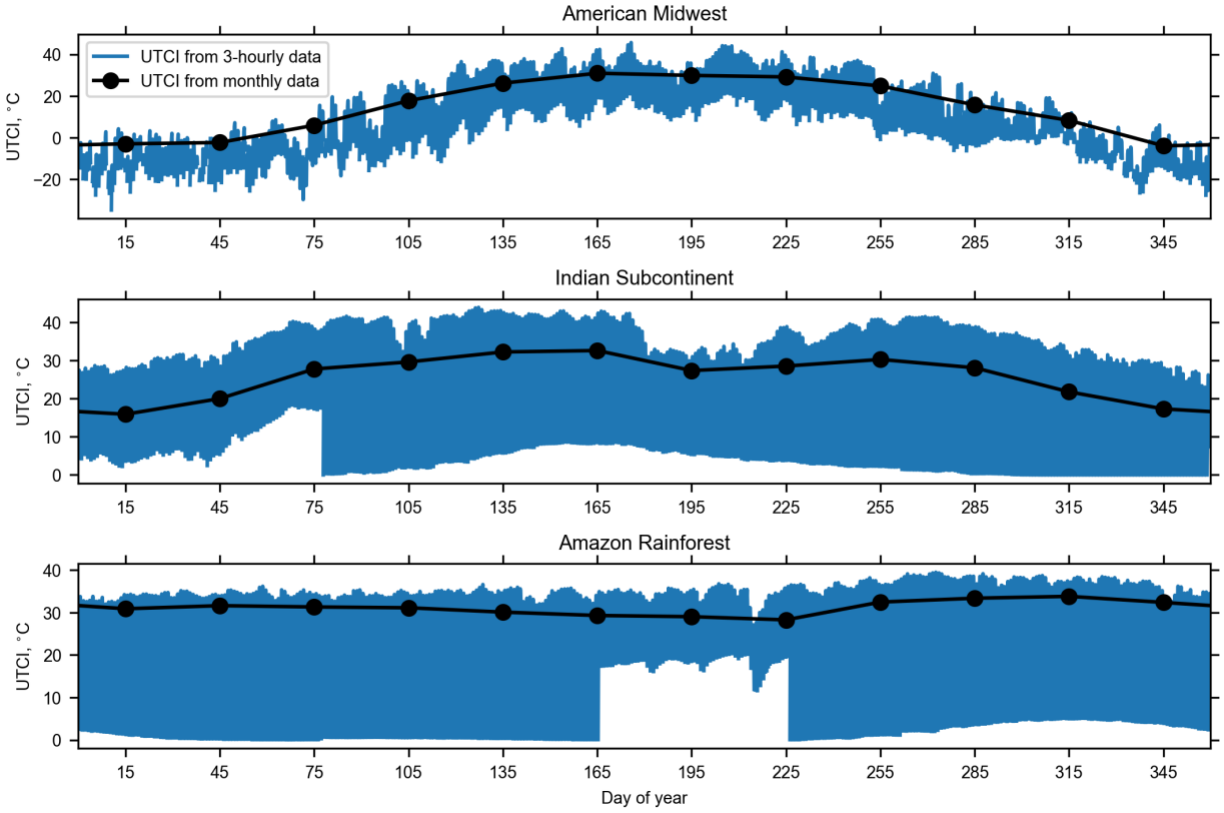

Extended Data Figure 4: Comparison of UTCI calculated using monthly mean climate data (black) with 3-hourly climate data (blue) for the three case study regions using the HadGEM2-ES climate model for the simulated year of 1985. HadGEM2-ES uses a 360-day calendar with 12 months of 30 days. As UTCI is only defined during daytime, the apparent sudden jumps in the 3-hourly data is due to the minimum value of UTCI changing with day length at various points in the year.

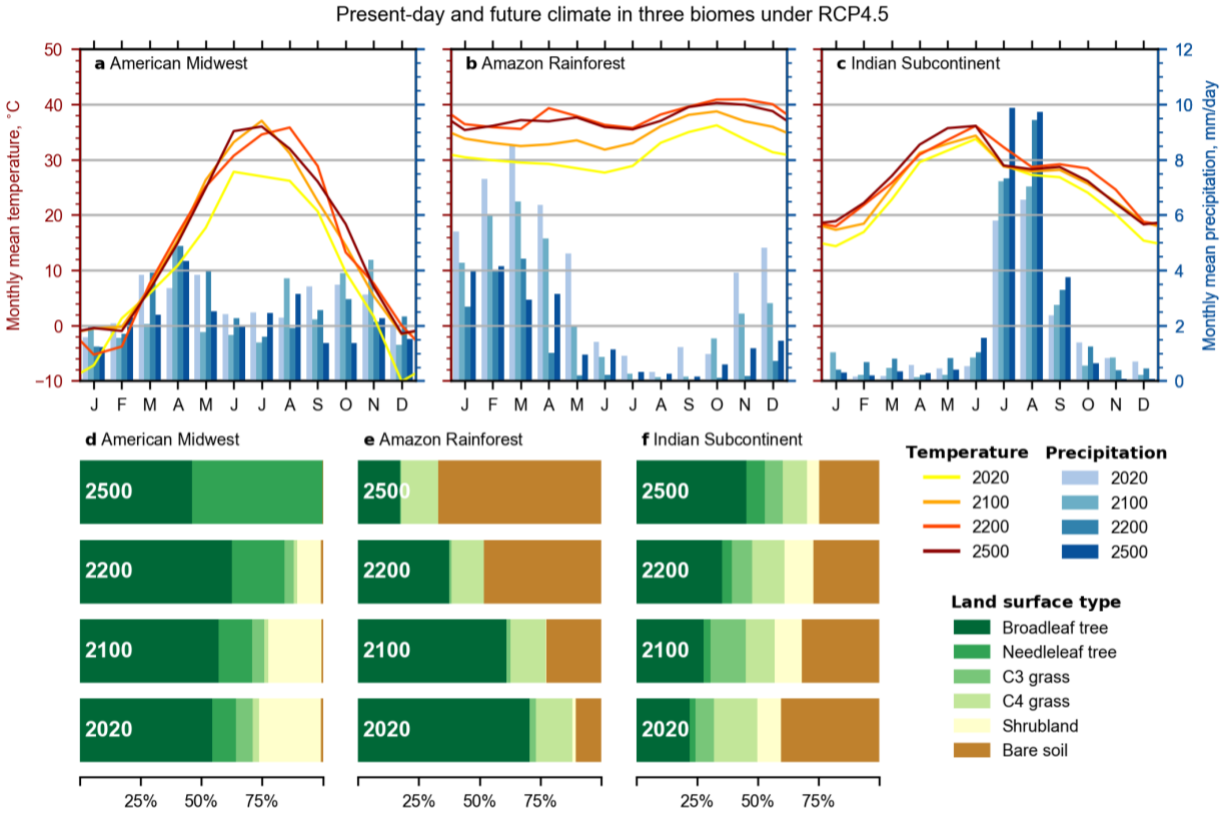

Extended Data Figure 5: Climatic indices for the three case study regions, under the RCP4.5 scenario in HadCM3. Monthly mean temperatures (°C; left axis) and precipitation (mm/day; right axis) in (a) the American Midwest, (b) Amazon and (c) Indian subcontinent. Land cover fractions, from the TRIFFID dynamic vegetation model in (d) American Midwest, (e) Amazon and (f) Indian subcontinent.

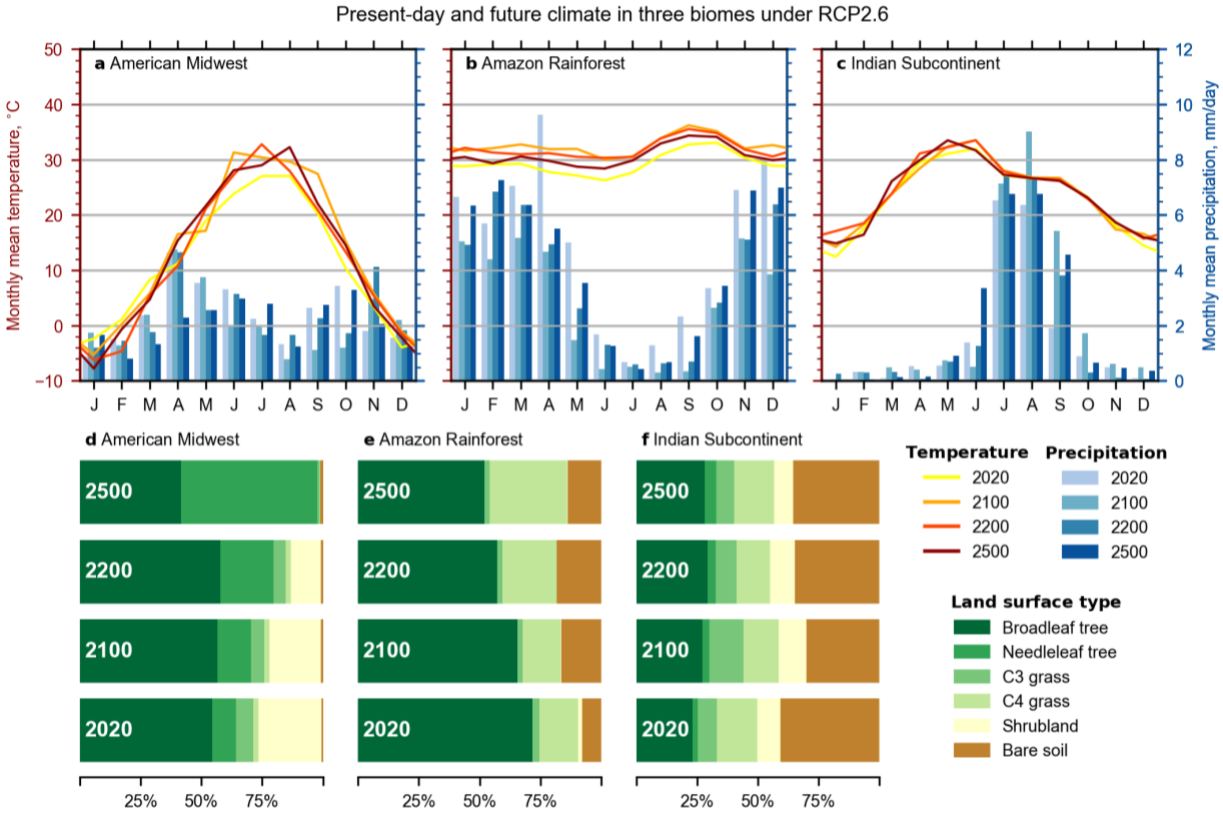

Extended Data Figure 6: Climatic indices for the three case study regions under the RCP2.6 scenario in HadCM3. Monthly mean temperatures (°C; left axis) and precipitation (mm/day; right axis) in (a) the American Midwest, (b) Amazon and (c) Indian subcontinent. Land cover fractions, from the TRIFFID dynamic vegetation model in (d) American Midwest, (e) Amazon and (f) Indian subcontinent.

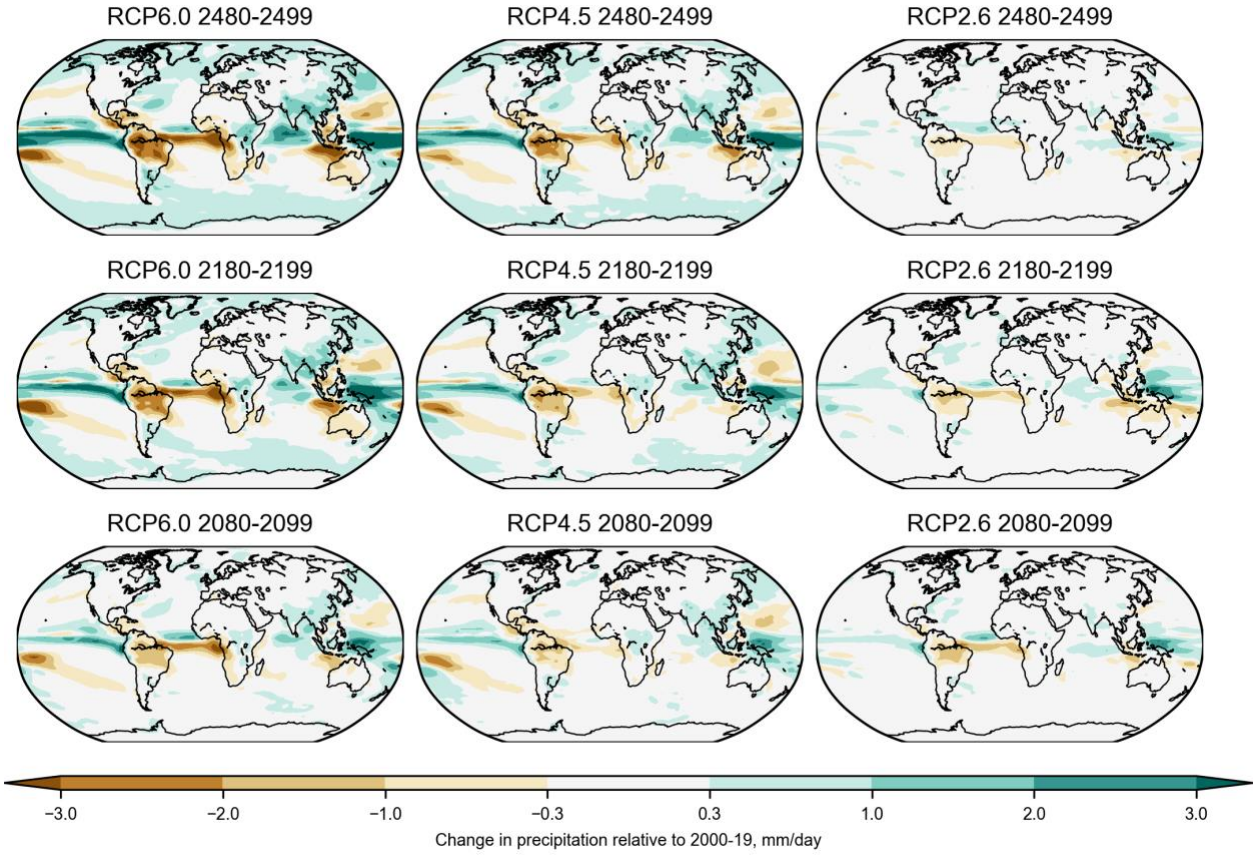

Extended Data Figure 7: Global changes in precipitation in 2100, 2200, and 2500 relative to the present day under RCPs 6.0 (left column), 4.5 (middle column), and 2.6 (right column) in mm/day.

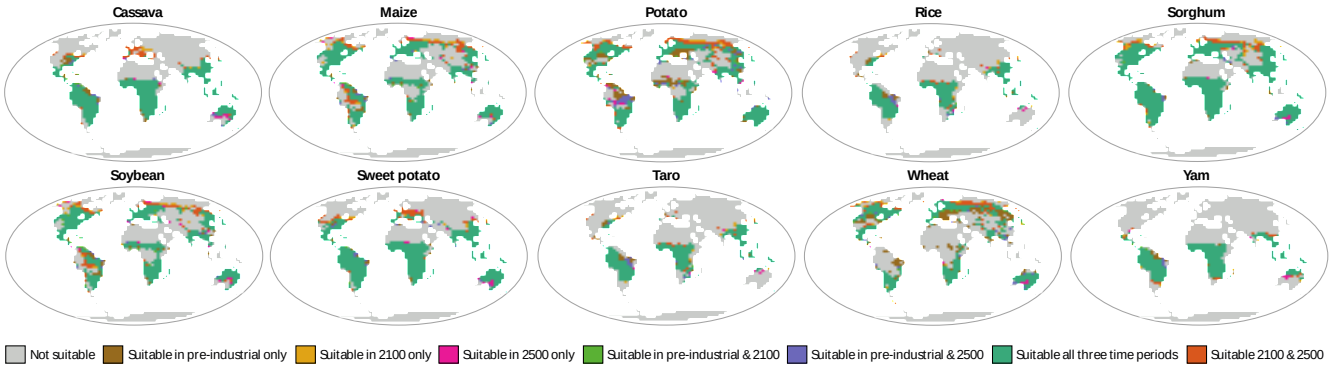

Extended Data Figure 8 Projections for crop suitability to 2100 and 2500 under the low RCP2.6 emission scenario. Modelling was based on temperature and precipitation requirements derived from the FAO[54], with crop growth length calibrated to the maps[55] (see Methods).

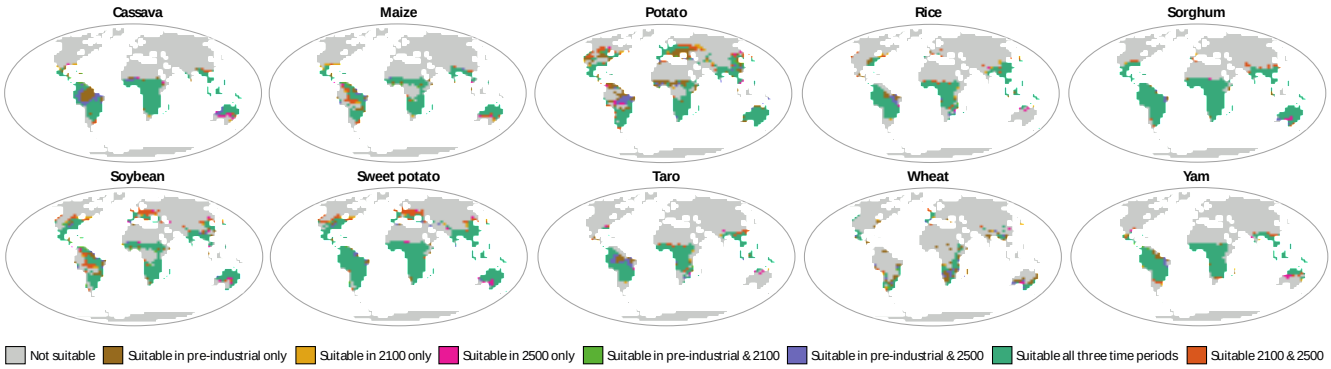

Extended Data Figure 9 Projections for crop suitability to 2100 and 2500 under the low RCP2.6 emission scenario. Modelling was based on temperature and precipitation requirements derived from the FAO[54], with crop growth length set to maximum number of months (see Methods).

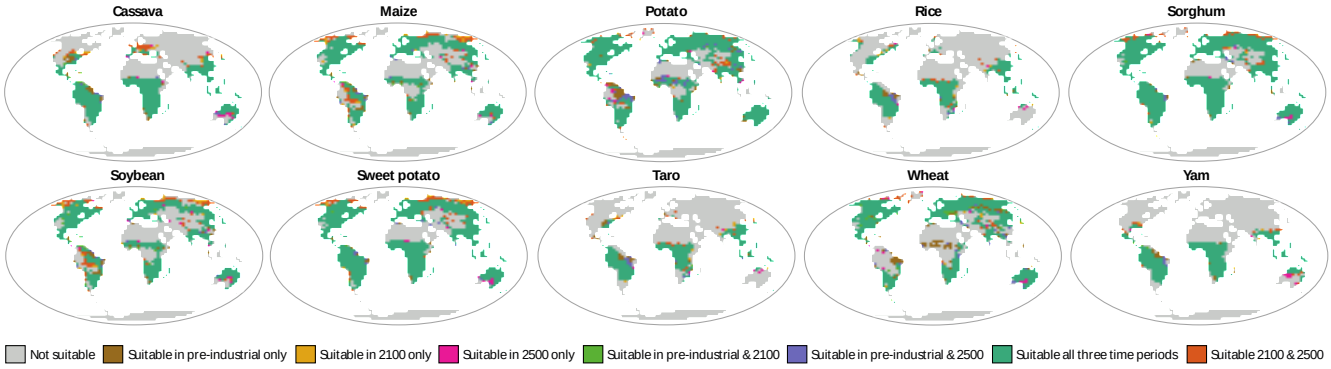

Extended Data Figure 10 Projections for crop suitability to 2100 and 2500 under the low RCP2.6 emission scenario. Modelling was based on temperature and precipitation requirements derived from the FAO[54], with crop growth length set to minimum number of months (see Methods).

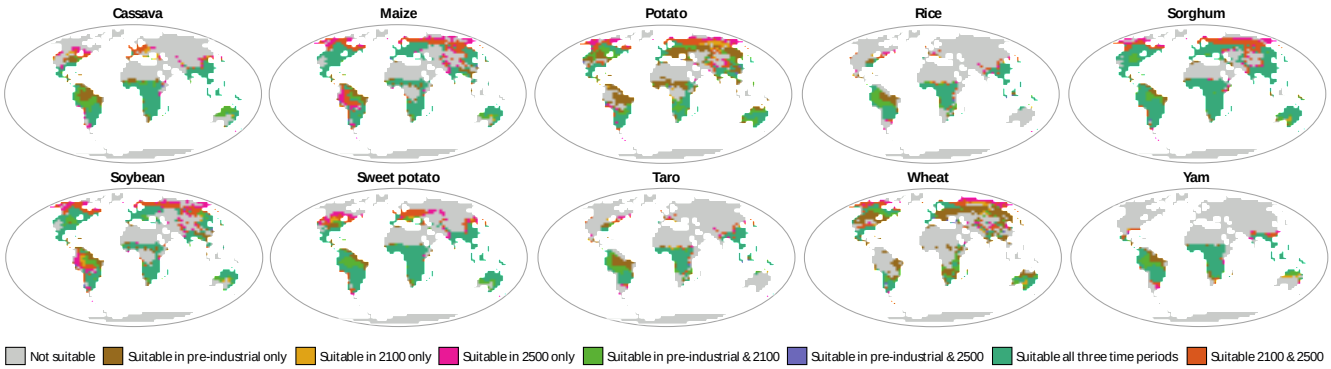

Extended Data Figure 11 Projections for crop suitability to 2100 and 2500 under the low RCP4.5 emission scenario. Modelling was based on temperature and precipitation requirements derived from the FAO[54], with crop growth length calibrated to the maps[55] (see Methods).

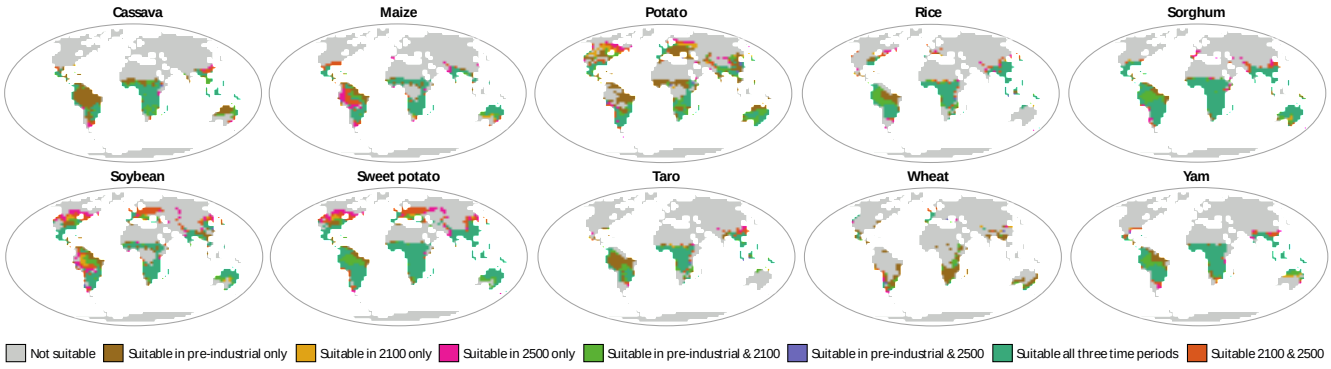

Extended Data Figure 12 Projections for crop suitability to 2100 and 2500 under the low RCP4.5 emission scenario. Modelling was based on temperature and precipitation requirements derived from the FAO[54], with crop growth length set to maximum number of months (see Methods).

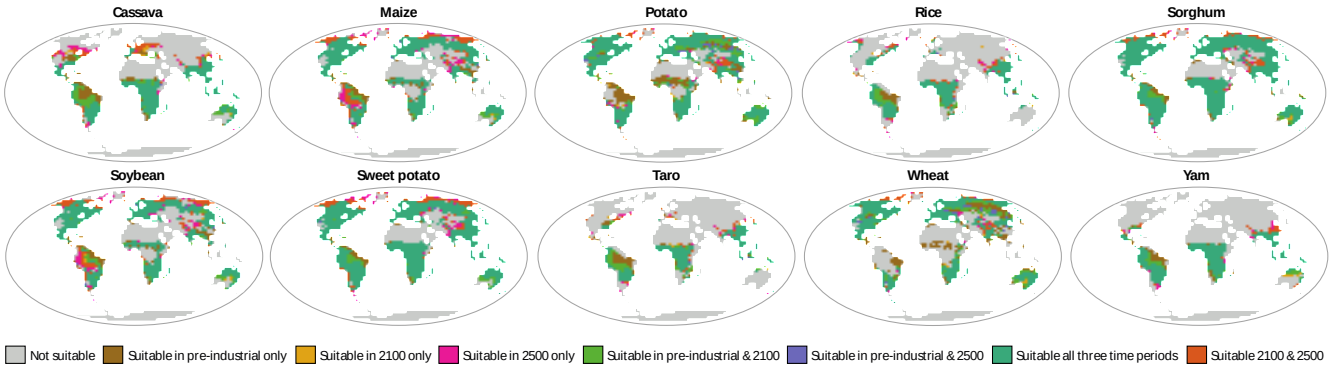

Extended Data Figure 13 Projections for crop suitability to 2100 and 2500 under the low RCP4.5 emission scenario. Modelling was based on temperature and precipitation requirements derived from the FAO[54], with crop growth length set to minimum number of months (see Methods).

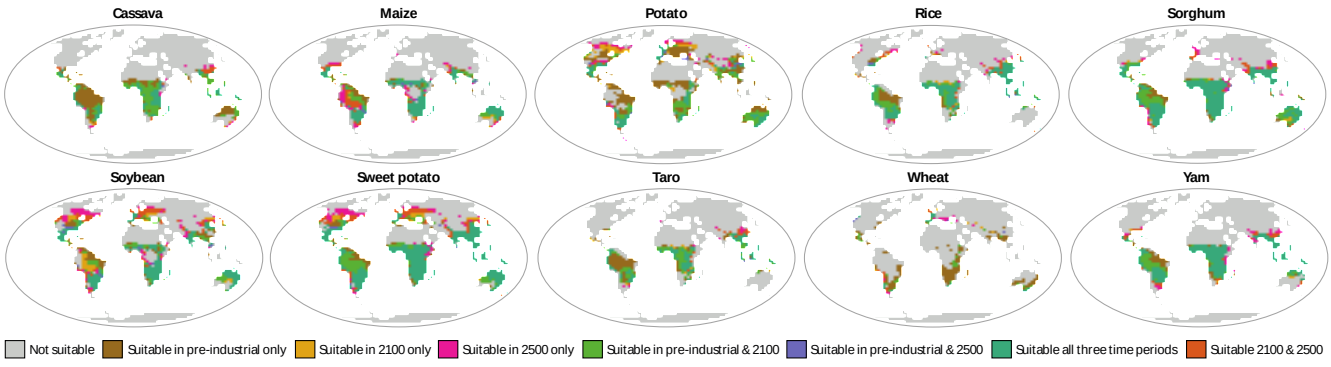

Extended Data Figure 14 Projections for crop suitability to 2100 and 2500 under the low RCP6.0 emission scenario. Modelling was based on temperature and precipitation requirements derived from the FAO[54], with crop growth length set to maximum number of months (see Methods).

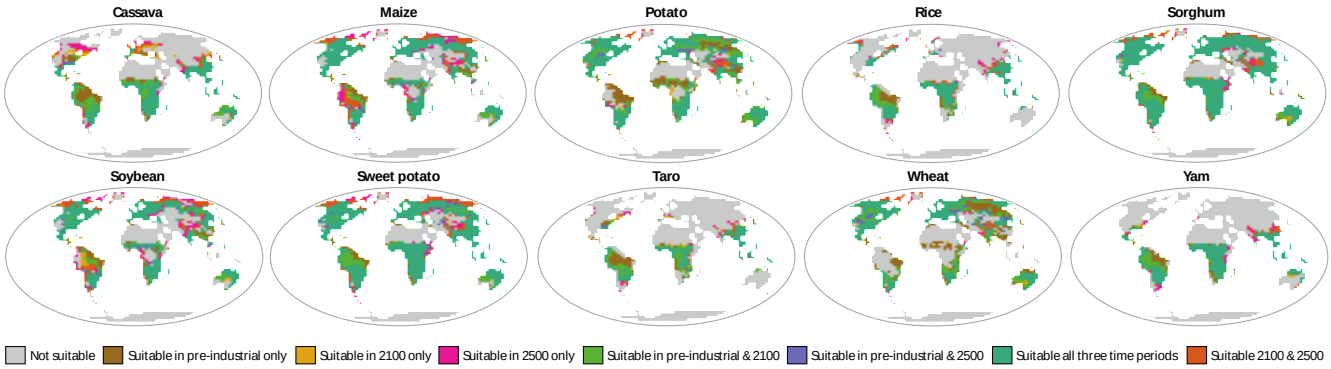

Extended Data Figure 15 Projections for crop suitability to 2100 and 2500 under the low RCP6.0 emission scenario. Modelling was based on temperature and precipitation requirements derived from the FAO[54], with crop growth length set to minimum number of months (see Methods).

Extended Data Table 1 Crop tolerance metadata used to calibrate crop model projections. Data derive from the Crop Ecological Requirements Database (Ecocrop) of FAO[54].

Species	Common Name	Min Absolute Temp (°C)	Max Absolute Temp (°C)	Rainfall Absolute Min (mm/year)	Rainfall Absolute Max (mm/year)	Crop cycle Min Months	Crop cycle Max Months	Crop cycle calibrated to crop growth globally
Manihot esculenta	Cassava	10	35	500	5000	6	12	7
Solanum tuberosum	Potato	7	30	250	2000	3	6	5
Glycine max	Soya Bean	10	38	450	1800	3	6	4
Oryza sativa	Rice	10	36	1000	4000	3	6	6
Ipomoea batatas	Sweet potato	10	38	350	5000	3	6	6
Sorghum bicolor var. sweet	Sorghum	8	40	300	3000	3	10	5
Colocasia esculenta	Taro	10	35	1000	4100	6	10	6
Triticum aestivum	Wheat	5	27	300	1600	3	9	5
Dioscorea alata	Yam	14	40	700	8000	8	10	10
Zea mays	Maize	10	47	400	1800	3	12	4

References

1. IPCC. Global Warming of 1.5°C. An IPCC Special Report on the impacts of global warming of 1.5°C above pre-industrial levels and related global greenhouse gas emission pathways, in the context of strengthening the global response to the threat of climate change, sustainable development, and efforts to eradicate poverty. (2019).

2. UNEP. The emissions gap report 2019. (United Nations Environment Programme [UNEP], 2019).
3. Clark, P. U. et al. Consequences of twenty-first-century policy for multi-millennial climate and sea-level change. Nature Clim Change **6**, 360–369 (2016).
4. Huntingford, C. et al. Simulated resilience of tropical rainforests to CO2-induced climate change. Nature Geosci **6**, 268–273 (2013).
5. Pearson, P. N. Climate: why set emissions timeline for 2100? Nature **580**, 456–456 (2020).
6. van Renssen, S. Looking past the horizon of 2100. Nat. Clim. Chang. **9**, 349–351 (2019).
7. Aggarwal, P., Vyas, S., Thornton, P. & Campbell, B. M. How much does climate change add to the challenge of feeding the planet this century? Environ. Res. Lett. **14**, 043001 (2019).
8. Ray, D. K. et al. Climate change has likely already affected global food production. PLoS ONE **14**, e0217148 (2019).
9. Adger, W. N. et al. Urbanization, Migration, and Adaptation to Climate Change. One Earth **3**, 396–399 (2020).
10. Chen, M. & Caldeira, K. Climate change as an incentive for future human migration. Earth Syst. Dynam. **11**, 875–883 (2020).
11. Zeebe, R. E., Ridgwell, A. & Zachos, J. C. Anthropogenic carbon release rate unprecedented during the past 66 million years. Nature Geoscience **9**, 325–329 (2016).
12. Burke, K. D. et al. Pliocene and Eocene provide best analogs for near-future climates. Proc Natl Acad Sci USA **115**, 13288–13293 (2018).
13. Pascale, S., Kapnick, S. B., Delworth, T. L. & Cooke, W. F. Increasing risk of another Cape Town "Day Zero" drought in the 21st century. Proc Natl Acad Sci USA 202009144 (2020) doi:10.1073/pnas.2009144117.

14. IPBES. Global assessment report on biodiversity and ecosystem services of the Intergovernmental Science-Policy Platform on Biodiversity and Ecosystem Services. https://ipbes.net/global-assessment (2019).
15. Ford, J. D. et al. Changing access to ice, land and water in Arctic communities. Nat. Clim. Chang. **9**, 335–339 (2019).
16. Riahi, K. et al. The Shared Socioeconomic Pathways and their energy, land use, and greenhouse gas emissions implications: An overview. Global Environmental Change **42**, 153–168 (2017).
17. van Vuuren, D. P. et al. The representative concentration pathways: an overview. Climatic Change **109**, 5–31 (2011).
18. Pedde, S. et al. Enriching the Shared Socioeconomic Pathways to co-create consistent multi-sector scenarios for the UK. Science of The Total Environment 143172 (2020) doi:10.1016/j.scitotenv.2020.143172.
19. O'Neill, B. C. et al. Achievements and needs for the climate change scenario framework. Nat. Clim. Chang. **10**, 1074–1084 (2020).
20. IPCC. Climate change 2013: the physical science basis: Working Group I contribution to the Fifth assessment report of the Intergovernmental Panel on Climate Change. (Cambridge University Press, 2014).
21. Meinshausen, M. et al. The shared socio-economic pathway (SSP) greenhouse gas concentrations and their extensions to 2500. Geosci. Model Dev. **13**, 3571–3605 (2020).
22. Zickfeld, K. et al. Long-Term Climate Change Commitment and Reversibility: An EMIC Intercomparison. Journal of Climate **26**, 5782–5809 (2013).
23. Forster, P. Half a century of robust climate models. Nature **545**, 296–297 (2017).
24. Gordon, C. et al. The simulation of SST, sea ice extents and ocean heat transports in a version of the Hadley Centre coupled model without flux adjustments. Climate Dynamics **16**, 147–168 (2000).

25. Cox, P. Description of the TRIFFID Dynamic Global Vegetation Model. (2001).
26. Braconnot, P. et al. Evaluation of climate models using palaeoclimatic data. Nature Clim Change **2**, 417–424 (2012).
27. McMahon, T. A., Peel, M. C. & Karoly, D. J. Assessment of precipitation and temperature data from CMIP3 global climate models for hydrologic simulation. Hydrol. Earth Syst. Sci. **19**, 361–377 (2015).
28. Randall, D. et al. Climate Models and Their Evaluation. in Climate Change 2007: The Physical Science Basis. Contribution of Working Group I to the Fourth Assessment Report of the Intergovernmental Panel on Climate Change (eds. Solomon, S. et al.) (Cambridge University Press, 2007).
29. Sherwood, S. C. et al. An Assessment of Earth's Climate Sensitivity Using Multiple Lines of Evidence. Rev. Geophys. **58**, (2020).
30. Schuur, E. A. G. et al. Climate change and the permafrost carbon feedback. Nature **520**, 171–179 (2015).
31. Brienen, R. J. W. et al. Long-term decline of the Amazon carbon sink. Nature **519**, 344–348 (2015).
32. Hausfather, Z. & Peters, G. P. Emissions – the 'business as usual' story is misleading. Nature **577**, 618–620 (2020).
33. Huntingford, C. et al. Towards quantifying uncertainty in predictions of Amazon 'dieback'. Phil. Trans. R. Soc. B **363**, 1857–1864 (2008).
34. Palmer, M. D., Harris, G. R. & Gregory, J. M. Extending CMIP5 projections of global mean temperature change and sea level rise due to thermal expansion using a physically-based emulator. Environ. Res. Lett. **13**, 084003 (2018).

35. Oppenheimer, M. et al. Chapter 4: Sea Level Rise and Implications for Low Lying Islands, Coasts and Communities. in IPCC Special Report on the Ocean and Cryosphere in a Changing Climate (eds. Pörtner, H.-O. et al.) (2019).
36. Sherwood, S. C. & Huber, M. An adaptability limit to climate change due to heat stress. Proceedings of the National Academy of Sciences **107**, 9552–9555 (2010).
37. Varghese, B. et al. Heatwave-related Mortality in Australia: Who's impacted the most? European Journal of Public Health **30**, ckaa165.377 (2020).
38. Diniz, F. R., Gonçalves, F. L. T. & Sheridan, S. Heat Wave and Elderly Mortality: Historical Analysis and Future Projection for Metropolitan Region of São Paulo, Brazil. Atmosphere **11**, 933 (2020).
39. Burillo, D., Chester, M. V., Pincetl, S. & Fournier, E. Electricity infrastructure vulnerabilities due to long-term growth and extreme heat from climate change in Los Angeles County. Energy Policy **128**, 943–953 (2019).
40. Villalba Sanchis, I., Insa Franco, R., Martínez Fernández, P., Salvador Zuriaga, P. & Font Torres, J. B. Risk of increasing temperature due to climate change on high-speed rail network in Spain. Transportation Research Part D: Transport and Environment **82**, 102312 (2020).
41. Anderson, R., Bayer, P. E. & Edwards, D. Climate change and the need for agricultural adaptation. Current Opinion in Plant Biology **56**, 197–202 (2020).
42. Mehrabi, Z. Food system collapse. Nat. Clim. Chang. **10**, 16–17 (2020).
43. Li, C. et al. Rapid Warming in Summer Wet Bulb Globe Temperature in China with Human-Induced Climate Change. Journal of Climate **33**, 5697–5711 (2020).
44. Im, E.-S., Pal, J. S. & Eltahir, E. A. B. Deadly heat waves projected in the densely populated agricultural regions of South Asia. Sci Adv **3**, (2017).
45. Pal, J. S. & Eltahir, E. A. B. Future temperature in southwest Asia projected to exceed a threshold for human adaptability. Nature Climate Change **6**, 197–200 (2016).

46. Błażejczyk, K. et al. An introduction to the Universal Thermal Climate Index (UTCI). Geogr. Pol. **86**, 5–10 (2013).
47. Stringer, L. C. et al. Adaptation and development pathways for different types of farmers. Environmental Science & Policy **104**, 174–189 (2020).
48. Sloat, L. L. et al. Climate adaptation by crop migration. Nat Commun **11**, 1243 (2020).
49. Zhang, Y., Wang, Y. & Niu, H. Spatio-temporal variations in the areas suitable for the cultivation of rice and maize in China under future climate scenarios. Science of The Total Environment **601–602**, 518–531 (2017).
50. Moore, F. The Fingerprint of Anthropogenic Warming on Global Agriculture. (2020) doi:10.31223/X5Q30Z.
51. King, M. et al. Northward shift of the agricultural climate zone under 21st-century global climate change. Sci Rep **8**, 7904 (2018).
52. Ceglar, A., Zampieri, M., Toreti, A. & Dentener, F. Observed Northward Migration of Agro-Climate Zones in Europe Will Further Accelerate Under Climate Change. Earth's Future **7**, 1088–1101 (2019).
53. Tigchelaar, M., Battisti, D. S., Naylor, R. L. & Ray, D. K. Future warming increases probability of globally synchronized maize production shocks. Proc Natl Acad Sci USA **115**, 6644–6649 (2018).
54. Food and Agriculture Organization (FAO). Crop Ecological Requirements Database (ECOCROP) [Offline as of February 2020]. FAO EcoCrop http://ecocrop.fao.org/ecocrop/srv/en/home (2016).
55. Monfreda, C., Ramankutty, N. & Foley, J. A. Farming the planet: 2. Geographic distribution of crop areas, yields, physiological types, and net primary production in the year 2000: GLOBAL CROP AREAS AND YIELDS IN 2000. Global Biogeochem. Cycles **22**, n/a-n/a (2008).

56. Crist, E., Mora, C. & Engelman, R. The interaction of human population, food production, and biodiversity protection. Science **356**, 260–264 (2017).
57. Kc, S. & Lutz, W. The human core of the shared socioeconomic pathways: Population scenarios by age, sex and level of education for all countries to 2100. Global Environmental Change **42**, 181–192 (2017).
58. Aguiar, A. P. D. et al. Co-designing global target-seeking scenarios: A cross-scale participatory process for capturing multiple perspectives on pathways to sustainability. Global Environmental Change **65**, 102198 (2020).
59. Mosby, I., Rotz, S. & Fraser, E. D. G. Uncertain harvest: the future of food on a warming planet. (University of Regina Press, 2020).
60. Bodirsky, B. L. et al. Global Food Demand Scenarios for the 21st Century. PLoS ONE **10**, e0139201 (2015).
61. Mehrabi, Z., Ellis, E. C. & Ramankutty, N. The challenge of feeding the world while conserving half the planet. Nature Sustainability **1**, 409–412 (2018).
62. Angel, J. R. et al. Chapter 21 : Midwest. Impacts, Risks, and Adaptation in the United States: The Fourth National Climate Assessment, Volume II. https://nca2018.globalchange.gov/chapter/21/ (2018) doi:10.7930/NCA4.2018.CH21.
63. Heckenberger, M. J., Christian Russell, J., Toney, J. R. & Schmidt, M. J. The legacy of cultural landscapes in the Brazilian Amazon: implications for biodiversity. Phil. Trans. R. Soc. B **362**, 197–208 (2007).
64. Friedlingstein, P. et al. Global Carbon Budget 2019. Earth Syst. Sci. Data **11**, 1783–1838 (2019).
65. Aikhenvald, A. Y. The languages of the Amazon. (Oxford University Press, 2015).
66. Sitch, S. et al. Evaluation of the terrestrial carbon cycle, future plant geography and climate-carbon cycle feedbacks using five Dynamic Global Vegetation Models (DGVMs):

UNCERTAINTY IN LAND CARBON CYCLE FEEDBACKS. Global Change Biology **14**, 2015–2039 (2008).

67. Poulter, B. et al. Robust dynamics of Amazon dieback to climate change with perturbed ecosystem model parameters. Global Change Biology (2010) doi:10.1111/j.1365-2486.2009.02157.x.
68. Cowling, S. A. et al. Contrasting simulated past and future responses of the Amazonian forest to atmospheric change. Phil. Trans. R. Soc. Lond. B **359**, 539–547 (2004).
69. Drijfhout, S. et al. Catalogue of abrupt shifts in Intergovernmental Panel on Climate Change climate models. Proc Natl Acad Sci USA **112**, E5777–E5786 (2015).
70. Mazdiyasni, O. et al. Increasing probability of mortality during Indian heat waves. Sci. Adv. **3**, e1700066 (2017).
71. Elson, J. C. Evaluation of personal cooling systems and simulation of their effects on human subjects using basic and advanced virtual environments. (Kansas State University, 2016).
72. Smith, J. C. Stillsuit. in The science of Dune: unauthorized exploration into the real science behind Frank Herbert's fictional universe (ed. Grazier, K. R.) 127–141 (BenBella Books, 2008).
73. Matthews, H. D., Gillett, N. P., Stott, P. A. & Zickfeld, K. The proportionality of global warming to cumulative carbon emissions. Nature **459**, 829–832 (2009).
74. Allen, M. R. et al. Warming caused by cumulative carbon emissions towards the trillionth tonne. Nature **458**, 1163–1166 (2009).
75. Rogelj, J., Forster, P. M., Kriegler, E., Smith, C. J. & Séférian, R. Estimating and tracking the remaining carbon budget for stringent climate targets. Nature **571**, 335–342 (2019).
76. Carton, W., Asiyanbi, A., Beck, S., Buck, H. J. & Lund, J. F. Negative emissions and the long history of carbon removal. WIREs Clim Change **11**, (2020).
77. Stevenson, H. Reforming global climate governance in an age of bullshit. Globalizations **18**, 86–102 (2021).

78. McLaren, D. & Markusson, N. The co-evolution of technological promises, modelling, policies and climate change targets. Nat. Clim. Chang. **10**, 392–397 (2020).

79. van der Geest, K. & Warner, K. Loss and damage in the IPCC Fifth Assessment Report (Working Group II): a text-mining analysis. Climate Policy **20**, 729–742 (2020).

80. Beardsworth, R. Climate science, the politics of climate change and futures of IR. International Relations **34**, 374–390 (2020).

81. Zabel, F., Putzenlechner, B. & Mauser, W. Global Agricultural Land Resources – A High Resolution Suitability Evaluation and Its Perspectives until 2100 under Climate Change Conditions. PLoS ONE **9**, e107522 (2014).

82. Chaplin-Kramer, R. et al. Global modeling of nature's contributions to people. Science **366**, 255–258 (2019).

83. Poeplau, C., Schroeder, J., Gregorich, E. & Kurganova, I. Farmers' Perspective on Agriculture and Environmental Change in the Circumpolar North of Europe and America. Land **8**, 190 (2019).

84. Hannah, L. et al. The environmental consequences of climate-driven agricultural frontiers. PLoS ONE **15**, e0228305 (2020).

85. Fraser, E. D. G. & Campbell, M. Agriculture 5.0: Reconciling Production with Planetary Health. One Earth **1**, 278–280 (2019).

86. Healy, S. et al. Planetary Food Commons and Postcapitalist Post-COVID Food Futures. Development (2020) doi:10.1057/s41301-020-00267-9.

87. Caniglia, G. et al. A pluralistic and integrated approach to action-oriented knowledge for sustainability. Nat Sustain (2020) doi:10.1038/s41893-020-00616-z.

88. Fazey, I. et al. Transforming knowledge systems for life on Earth: Visions of future systems and how to get there. Energy Research & Social Science **70**, 101724 (2020).

89. Ford, J. D. et al. The Resilience of Indigenous Peoples to Environmental Change. One Earth **2**, 532–543 (2020).
90. Nursey-Bray, M., Palmer, R., Smith, T. F. & Rist, P. Old ways for new days: Australian Indigenous peoples and climate change. Local Environment **24**, 473–486 (2019).
91. Lam, D. P. M. et al. Indigenous and local knowledge in sustainability transformations research: a literature review. E&S **25**, art3 (2020).
92. Lynge, A. & Stenbaek, M. Inuit Arctic Policy. (2016).
93. Millward-Hopkins, J., Steinberger, J. K., Rao, N. D. & Oswald, Y. Providing decent living with minimum energy: A global scenario. Global Environmental Change **65**, 102168 (2020).
94. O'Neill, D. W., Fanning, A. L., Lamb, W. F. & Steinberger, J. K. A good life for all within planetary boundaries. Nat Sustain **1**, 88–95 (2018).
95. UNFCCC. Adoption of the Paris Agreement. http://unfccc.int/resource/docs/2015/cop21/eng/l09r01.pdf (2015).
96. Roelfsema, M. et al. Taking stock of national climate policies to evaluate implementation of the Paris Agreement. Nat Commun **11**, 2096 (2020).
97. Dosio, A., Mentaschi, L., Fischer, E. M. & Wyser, K. Extreme heat waves under 1.5 °C and 2 °C global warming. Environ. Res. Lett. **13**, 054006 (2018).
98. Schleussner, C.-F. et al. Differential climate impacts for policy-relevant limits to global warming: the case of 1.5 °C and 2 °C. Earth Syst. Dynam. **7**, 327–351 (2016).
99. Vrontisi, Z. et al. Enhancing global climate policy ambition towards a 1.5 °C stabilization: a short-term multi-model assessment. Environ. Res. Lett. **13**, 044039 (2018).
100. Muiderman, K., Gupta, A., Vervoort, J. & Biermann, F. Four approaches to anticipatory climate governance: Different conceptions of the future and implications for the present. WIREs Clim Change **11**, (2020).

101. Harrison, P. A., Jäger, J., Frantzeskaki, N. & Berry, P. Understanding high-end climate change: from impacts to co-creating integrated and transformative solutions. Reg Environ Change **19**, 621–627 (2019).
102. Marien, M. The future of human benefit knowledge: Notes on a World Brain for the 21st century. Futures **39**, 955–962 (2007).
103. Robinson, K. S. The Ministry for the Future. (Orbit Books, 2020).
104. Bennett, E. M. Changing the agriculture and environment conversation. Nat Ecol Evol **1**, 0018 (2017).
105. Leach, N. J. et al. Current level and rate of warming determine emissions budgets under ambitious mitigation. Nature Geosci **11**, 574–579 (2018).
106. Taylor, K. E., Stouffer, R. J. & Meehl, G. A. An Overview of CMIP5 and the Experiment Design. Bulletin of the American Meteorological Society **93**, 485–498 (2012).
107. Cox, P. M. et al. The impact of new land surface physics on the GCM simulation of climate and climate sensitivity. Climate Dynamics **15**, 183–203 (1999).
108. Essery, R. L. H., Best, M. J., Betts, R. A., Cox, P. M. & Taylor, C. M. Explicit Representation of Subgrid Heterogeneity in a GCM Land Surface Scheme. Journal of Hydrometeorology **4**, 530–543 (2003).
109. Valdes, P. J. et al. The BRIDGE HadCM3 family of climate models: HadCM3@Bristol v1.0. Geosci. Model Dev. **10**, 3715–3743 (2017).
110. Hersbach, H. et al. The ERA5 global reanalysis. Q.J.R. Meteorol. Soc. **146**, 1999–2049 (2020).
111. Cox, P. M., Huntingford, C. & Harding, R. J. A canopy conductance and photosynthesis model for use in a GCM land surface scheme. Journal of Hydrology **212–213**, 79–94 (1998).
112. Meinshausen, M. et al. The RCP greenhouse gas concentrations and their extensions from 1765 to 2300. Climatic Change **109**, 213–241 (2011).

113. Riahi, K. et al. RCP 8.5—A scenario of comparatively high greenhouse gas emissions. Climatic Change **109**, 33–57 (2011).

114. Kuhlbrodt, T. & Gregory, J. M. Ocean heat uptake and its consequences for the magnitude of sea level rise and climate change. Geophys. Res. Lett. **39**, (2012).

115. Giorgi, F. & Francisco, R. Uncertainties in regional climate change prediction: a regional analysis of ensemble simulations with the HADCM2 coupled AOGCM. Climate Dynamics **16**, 169–182 (2000).

116. Jendritzky, G., de Dear, R. & Havenith, G. UTCI—Why another thermal index? Int J Biometeorol **56**, 421–428 (2012).

117. Broede, P. UTCI, Version a 0.002, October 2009. (2009).

118. Di Napoli, C., Hogan, R. J. & Pappenberger, F. Mean radiant temperature from global-scale numerical weather prediction models. Int J Biometeorol **64**, 1233–1245 (2020).

119. Kántor, N. & Unger, J. The most problematic variable in the course of human-biometeorological comfort assessment — the mean radiant temperature. Open Geosciences **3**, (2011).

120. Liu, B. Y. H. & Jordan, R. C. The interrelationship and characteristic distribution of direct, diffuse and total solar radiation. Solar Energy **4**, 1–19 (1960).

121. Erbs, D. G., Klein, S. A. & Duffie, J. A. Estimation of the diffuse radiation fraction for hourly, daily and monthly-average global radiation. Solar Energy **28**, 293–302 (1982).

122. Porfirio, L. L., Newth, D., Harman, I. N., Finnigan, J. J. & Cai, Y. Patterns of crop cover under future climates. Ambio **46**, 265–276 (2017).

123. Abdallah, C. & Jaafar, H. Data set on current and future crop suitability under the Representative Concentration Pathway (RCP) 8.5 emission scenario for the major crops in the Levant, Tigris-Euphrates, and Nile Basins. Data in Brief **22**, 992–997 (2019).

124. Ramankutty, N. & Foley, J. A. Characterizing patterns of global land use: An analysis of global croplands data. Global Biogeochem. Cycles **12**, 667–685 (1998).

125. Leff, B., Ramankutty, N. & Foley, J. A. Geographic distribution of major crops across the world. Global Biogeochem. Cycles **18**, n/a-n/a (2004).

126. Crop adaptation to climate change. (Wiley-Blackwell, 2011).

127. Millington, J. D. A. & Wainwright, J. Agent-based modelling and landscape change. (2016).

128. The Climate-Smart Agriculture Papers: Investigating the Business of a Productive, Resilient and Low Emission Future. (Springer International Publishing, 2019). doi:10.1007/978-3-319-92798-5.

129. Egbebiyi, T. S., Crespo, O. & Lennard, C. Defining Crop–climate Departure in West Africa: Improved Understanding of the Timing of Future Changes in Crop Suitability. Climate **7**, 101 (2019).

130. Manners, R., Varela-Ortega, C. & van Etten, J. Protein-rich legume and pseudo-cereal crop suitability under present and future European climates. European Journal of Agronomy **113**, 125974 (2020).

131. Thomson, A. M. et al. RCP4.5: a pathway for stabilization of radiative forcing by 2100. Climatic Change **109**, 77–94 (2011).

132. Masui, T. et al. An emission pathway for stabilization at 6 Wm−2 radiative forcing. Climatic Change **109**, 59–76 (2011).

133. R Core Team. R: A language and environment for statistical computing. (R Foundation for Statistical Computing, 2020).

134. Masante, D. bnspatial: Spatial Implementation of Bayesian Networks and Mapping. R package version 1.1.1. (2020).

135. Hijmans, R. J. raster: Geographic Data Analysis and Modeling. R package version 3.0-7. (2019).

136. Bivand, R. & Rundel, C. rgeos: Interface to Geometry Engine - Open Source ('GEOS'). R package version 0.5-2. (2019).

137. Raymundo, R. et al. Climate change impact on global potato production. European Journal of Agronomy **100**, 87–98 (2018).

138. Najafi, E., Devineni, N., Khanbilvardi, R. M. & Kogan, F. Understanding the Changes in Global Crop Yields Through Changes in Climate and Technology. Earth's Future **6**, 410–427 (2018).

139. You, L., Wood, S., Wood-Sichra, U. & Wu, W. Generating global crop distribution maps: From census to grid. Agricultural Systems **127**, 53–60 (2014).

140. Jackson, N. D., Konar, M., Debaere, P. & Estes, L. Probabilistic global maps of crop-specific areas from 1961 to 2014. Environ. Res. Lett. **14**, 094023 (2019).

141. Mbow, C. et al. Food Security. in Climate Change and Land: an IPCC special report on climate change, desertification, land degradation, sustainable land management, food security, and greenhouse gas fluxes in terrestrial ecosystems (eds. Shukla, P. R. et al.) (In press, 2019).

Acknowledgements

This research forms part of the Refugia of Futures Past project funded through the White Rose Collaboration Fund. The climate modelling was undertaken on ARC3, part of the High Performance Computing facilities at the University of Leeds, UK. The authors are most grateful to Tom J. Webb, Deborah Sporton, Claudia Di Napoli, and David R Williams for their feedback at various stages of this work.

Author contributions

The research was designed by C.L., E.E.S., T.A, A.P.B., A.B., A.M.D., D.J.H., R.M., L.C.S., P.O., D.J.H. and C.S. conducted the climate and vegetation modelling. E.E.S. conducted the crop modelling and analysis. C.S. conducted the heat stress modelling. C.L., A.B., J.M., L.C.S., R.M., and P.O. assessed the human implications of modelling results. C.L. and E.E.S. wrote the initial draft of the paper, and all authors contributed to revisions.

Competing interest declaration

The authors declare no competing interests.

Data availability

The Ecocrop data supporting the crop model findings were freely available from the Food and Agriculture Organisation Ecocrop database http://ecocrop.fao.org/ecocrop/ until February 2020 (December 2020 website message states, "Service temporarily unavailable"). The authors declare these data are available within the paper and its supplementary information files.

Supplementary Information

Supplementary information is available for this paper.

Corresponding author

Correspondence and requests for materials should be addressed to Christopher Lyon, c.lyon@leeds.ac.uk.